UC San Diego

UC San Diego Electronic Theses and Dissertations

Title

Engineering Microvascular Interventions for Hemorrhage, Neoplasia, and Inflammatory Disease

Permalink

Author

Jani, Vinay Pinakin

Publication Date

2021

Peer reviewed|Thesis/dissertation

UNIVERSITY OF CALIFORNIA SAN DIEGO

Engineering Microvascular Interventions for Hemorrhage, Neoplasia, and Inflammatory Disease

A Thesis submitted in partial satisfaction of the
requirements for the degree
Master of Science

in

Bioengineering

by

Vinay P. Jani

Committee in charge:

Professor Pedro Cabrales, Chair
Professor Francisco Contijoch
Professor Geert Schmid-Schoenbein

2021

The Thesis of Vinay P. Jani is approved, and it is acceptable in quality and form for publication on microfilm and electronically.

University of California San Diego

2021

DEDICATION

To my parents, Pinakin and Chetna Jani, who always helped me achieve anything

I wanted to do, and my brother, Vivek Jani, who taught me that in research just

like life it is important to never give up.

EPIGRAPH

It has long been an axiom of mine that

the little things are infinitely the most important.

-Sir Arthur Conan Doyle

TABLE OF CONTENTS

LIST OF FIGURES

LIST OF TABLES

ACKNOWLEDGEMENTS

VITA

2019	B. S. in Chemistry *cum laude*, University of California San Diego
2020-2021	Graduate Teaching Assistant, University of California San Diego
2021	M. S. in Bioengineering, University of California San Diego

PUBLICATIONS

Jani, VP. Lucas, A. Jani, V. Munoz, CJ. Williams, AT. Yalcin, O. Cabrales, P. Numerical Model for the Determination of Erythrocyte Mechanical Properties and Wall Shear Stress in Vivo from Intravital Microscopy. Frontiers of Physiology. 2020.

Jani, V. Jani, VP. Munoz, CJ. Govender, K. Williams, AT. Cabrales, P. Application of Negative Interstitial Pressure Improves Functional Capillary Density in Hemorrhagic Shock. Physiological Reports. 2021.

Jani, V. Robert Asaro. Bryan Oronsky, Cabrales, P. RRx-001 increases erythrocyte preferential adhesion to the tumor vasculature. International Journal of Medical Sciences. 2021.

Jani, V. P, Friedman, J. M., and Cabrales, P. (2021). NO Nanoparticles Reduce Inflammation in a Small Animal Model of ARDS. (In Progress)

ABSTRACT OF THE THESIS

Engineering Microvascular Interventions for Hemorrhage, Neoplasia, and Inflammatory Disease

by

Vinay P. Jani

Master of Science in Bioengineering

University of California San Diego, 2021

Professor Pedro Cabrales, Chair

There has been a growing body of evidence that impaired microvascular perfusion is an indicator for mortality in critical patients. However, there are limited clinical microvascular therapeutics targets. The objective of this thesis is to investigate and intervene upon microvascular disease found in hemorrhagic shock, neoplasia, and inflammation concurrent with acute respiratory distress (ARDS). Chapter one of this thesis focuses on engineering an intervention to improve microvascular perfusion by leveraging the Starling forces in capillaries. Specifically, we designed and implemented a device for the application of negative pressure to reduce tissue interstitial pressure, which transiently increased functional capillary density after hemorrhagic

shock, a known metric for microvascular perfusion, without the need for volume resuscitation. Chapter two aims on engineering red blood cells to target the tumor microcirculation and microenvironment. Specifically, we studied red blood cells as a delivery vehicle for RRx-001, an anti-cancer agent, and altered their biomechanics, by selectively inducing tumor adhesion in the tumor microenvironment. This increase in adhesion had an anti-neoplastic effect, with our study showing a 40% decrease in tumor size. In chapter three, we engineered a new intervention for altering microvascular inflammation as seen in the acute respiratory distress syndrome (ARDS). Specifically, we aerosolized Nitric Oxide releasing nanoparticles (NO-nps) to mice suffering of ARDS and found a reduction in peripheral neutrophils, indicative of reduced inflammation. As demonstrated, engineering interventions to improve microvascular perfusion shows great potential as a therapeutic target for a broad range of pathophysiologies, including hemorrhagic shock, cancer, and ARDS.

Introduction

Background - The Microcirculation. The microcirculation encompasses small vessels, including arterioles and venules, with diameters less than 100 μm, and capillaries, with diameter between 5-8 μm [1]. In the normal physiology, the microvasculature is responsible for the delivery of oxygen and transport of nutrients and blood borne hormones to the parenchyma [2]. As such, microvessels dynamically responds to the changes in tissue O_2 demand via changing vascular tone, and by the activity of pericytes, cells responsible for capillary flow regulation [3]. Importantly, dynamic changes in vascular tone are mediated by vasoactive small molecules, including nitric oxide, which has recently been leveraged for its therapeutic potential [4].

Due to the close relationship between the microcirculation and parenchymal cells, the term "vasculo parenchymal communication" is often used to describe the paramount importance of the microcirculation response to the parenchymal cells' ever-changing needs [5]. In normal circumstances, vascular release of nitric oxide induces vasodilation and reduces inflammation, allowing for normal parenchymal function [6]. However, in diseased or stressed states, the endothelium releases reactive oxygen species, which is thought to be integral to microcirculatory dysfunction and subsequent dysregulated vascular tone and inflammation, leading to thrombosis and cellular dysfunction [7, 8]. More recently, primary endothelial dysfunction and loss of reactivity to vasoactive substances has also been cited as responsible for essential hypertension and diabetic microvascular disease, highlighting the importance of the microcirculation clinically [9].

Classically, the microcirculation has been of clinical interest only because of its role in regulating systemic hemodynamics, namely arterial control of mean arterial pressure and venular control of venous return to the heart [10]. More recently, however, it has been argued that the microcirculation is one of the most integral parts of the cardiovascular system, provided its direct communication with the parenchyma [2]. As alluded to above, microvascular dysfunction has been associated with a variety of clinical pathologies with variable clinical presentation, including

but not limited to Systemic Lupus Erythematosus, (SLE) Chagas Disease, and vascular dementia [5]. Moreover, the impact of microvessels on inflammation, cell to cell interaction, and tissue edema is greatly underappreciated. Thus, the clinical relevance of the microcirculation in systemic infectious, inflammatory, rheumatologic, and cardiovascular disease will continue to expand, and may provide insight into novel therapies with broad indications.

In more acute settings, microvascular function has been shown to be a key predictor of outcomes, including ICU duration, ventilator time, post ICU morbidity, and mortality, in many critically ill patients. In fact, microvascular function was shown to be a significant prognosticator for morbidity and mortality in the case of COVID-19 [11, 12]. Many disorders present with or are caused by underlying hypoxia in tissues; however, their effects on microvascular are quite variable and vital for prognostication, as the microcirculation is a significant regulator of oxygen transport [13, 14]. Furthermore, hypoxia on its own has deleterious effects on microvascular function, which has significant implications physiologically [14]. It therefore only follows that study of the microvasculature will be impactful in understanding a broad range of disease models and will be vital for the development of broad treatment strategies that will improve outcomes in critically ill patients. This thesis will leverage the distinct nature of the microvascular changes in three different pathologies: hemorrhagic shock, neoplasia, and acute respiratory distress syndrome (ARDS) and engineer specific interventions that selectively improve microvascular function and thus tissue perfusion, as summarized in Figure 0.1.

The Microcirculation in Hemorrhagic Shock. Chapter 1 of this thesis seeks to leverage the Starling Forces and phenomenological properties of microvascular fluid transport to transiently improve capillary perfusion during hemorrhagic shock. Unlike in septic shock, where the inflammatory response can cause acute damage to the vasculature and surrounding parenchyma, hypovolemic shock, of which hemorrhagic shock is a subtype, is a problem with decreased intravascular volume such that the oxygen requirements of the tissues cannot be met [15, 16]. This chapter will specifically focus on hemorrhagic shock, which does not include other forms

Hemorrhagic Shock

Problem
Impaired microvascular perfusion even after correction of systemic hemodynamics

→

Objective
Transiently increase microvascular perfusion without volume resuscitation

→

Solution
Negative Pressure Chamber

Neoplasia

Problem
Abnormal and inefficent tumor microvasculature prevents effective drug delivery

→

Objective
Leverage the unique inflammatory signature for improved drug delivery by shunting flow through more efficient blood vessels

→

Solution
RRx-001 treated Red Blood Cells

Acute Respiratory Distress Syndrome (ARDS)

Problem
High permeability pulmonary edema and acute hypoxemic respiratory failure

→

Objective
Along with BIPAP, treat underlying epithelial injury and systemic inflammation responsible for disease pathogenesis

→

Solution
Nitric Oxide releasing Nanoparticles

Figure 0.1: Overview of the Thesis

of hypovolemic shock where intravascular volume can decrease such as dehydration [17]. Such a distinction is important given the acute nature of hemorrhagic shock and subsequent acute compensatory mechanisms that exist to maintain mean arterial pressure and thus perfusion. Specifically, in hemorrhagic shock, decreased oxygenation of tissues from blood loss induces a metabolic shift to anaerobic respiration in systemic tissue, thereby resulting in a buildup of lactic acid and subsequent metabolic acidosis [18]. Importantly, severe metabolic acidosis in hemorrhagic shock results in loss of peripheral vasoconstriction and death.

Systemically, hemorrhagic shock is known to increase cardiac contractility and heart rate, both of which compensate for loss of cardiac output, and systemic vascular resistance from baroreceptor activation, which leads to sympathetic nervous system activation and subsequent peripheral vasoconstriction [17]. Importantly, vasoconstriction of arterioles and venous system

have markedly different functions. For arterioles, vasoconstriction increases vascular resistance, while vasoconstriction of the venules increases venous return to the myocardium to increase preload. Moreover, peripheral vasoconstriction leads to blood being diverted from non-critical organs to more critical ones such as the heart and brain. This can prolong the viability of essential organs but can also lead to an increase in hypoxemia in non-essential organs, which can lead to acidosis, and tissue death [17]. Transfusion can help correct systemic hemodynamics in cases of hemorrhagic shock, but in cases of severe hemorrhagic shock there is still widespread organ failure even with transfusion [14, 19]. It is well known that even with correction of systemic hemodynamics from transfusion, microcirculatory perfusion is often compromised in these cases [14]. Moreover, transfusion may be a slow process in cases of emergent hemorrhagic shock due to limitations in the availability of blood and lack of venous access due to depleted intravascular volume

This chapter offers an innovative solution to the problem of decreased microvascular perfusion during hemorrhagic shock and offers a means to "buy time" for patients until transfusion may be available. To accomplish this, we have designed a system that exploits the Starling Forces and microvascular biomechanics via a negative pressure chamber. Our negative pressure chamber lowers the intravascular pressure resulting in a subsequent increase in perfusion secondary to increased capillary flow [20]. Our approach exploits the mechanics and normal endothelial function of capillaries and the surrounding microvasculature. all of which are not explicitly compromised during hemorrhagic shock contrary to infection and sepsis.

The Tumor Microvasculature. Chapter 2 focuses on engineering red blood cells to preferentially adhere to the tumor microvasculature, which will not only decrease tumor viability, but also induce chemo- and radio-sensitization of the tumor itself. The tumor microvasculature is biologically unique and is characterized by pockets of hypoxia and friable and tortious vasculature due to increased vascular endothelial growth factors, reduced blood flow, and ischemia [21]. Moreover, in the tumor microenvironment, an increase of circulating inflammatory factors, such

4

as tumor necrosis factor alpha (TNF-α), induces a unique environment, which can be exploited.

The inflammatory milieu of the tumor microcirculation coupled with pockets of hypoxia and ischemia lead to increased phospholipid phosphatidyl serine receptor expression on the endothelium. In older and sickled red bloods, phospholipid phosphatidyl serine expression is known to increase due to an increase of hemoglobin oxidation [22, 23]. This chapter aims to exploit these historical findings and engineers RBCs with RRx-001, a known anti-tumor agent, to take advantage of phospholipid phosphatidyl serine receptors within the tumor microvasculature as a potential therapeutic target [24, 25, 26]. Important to the radio- and chemo-sensitization seen with RRx-001 RBCs is the hypothesis that RBCs that occlude or decrease flow through less efficient more inflamed vessels in the tumor allow for shunting of flow to more efficient tumor vessels. This study also takes advantage of the RBC's ability to scavenge nitric oxide as RRx-001 binds to a cysteine residue on the beta chain of hemoglobin which prevents nitric oxide adduction, thereby leading to hemoglobin oxidation and PS expression and also tumor vascular endothelial oxidation [27, 28]. Thus, this study not only takes advantage of the RBC and its role in the microcirculation, but also the impact of nitric oxide and its effects on microvascular function.

The Microcirculation in ARDS.Chapter 3 will focus on targeting the microvascular dysfunction in acute respiratory distress syndrome (ARDS) by testing engineered approaches for NO delivery, namely NO releasing nanoparticles [29, 30, 31]. In this chapter, ARDS was induced by lipopolysaccharide administration, modeling gram negative bacterial pneumonia. Pathologically, ARDS is classically thought of in three distinct phases: 1. Diffuse alveolar damage (DAD) causing alveolar edema, 2. Proliferative phase, and 3. Fibrotic Phase. Clincially, ARDS is hallmarked by low oxygenation and non-compliant and stiff lungs in the absence of cardiogenic pulmonary edema [31]. Moreover, ARDS severity is defined by PaO2 to FiO2, the ratio of arterial blood gas O2 to inspired air. With respect to disease etiology, ARDS from pathogenic infection results from lung injury secondary to inflammatory pathways induced by infection. These inflammatory pathways can damage alveoli, which increases endothelial and epithelial permeability. Increased

permeability results in accumulation of fluid in the extravascular space, which increasing the work needed for expiration and impaired gas exchange leading to hypoxemia [32].

ARDS also is associated with capillary endothelial injury; critical to this injury is the role of nitric oxide (NO) [4]. In ARDS, there is a decreased ratio of nitric oxide to reactive oxygen species, which leads to M1 macrophage activation and RBC membrane damage [31]. Importantly, RBC damage results in hemoglobin release, which results in increased hemoglobin NO scavenging and a subsequent increase in oxidation and microvascular dysfunction. Moreover, increased NO induces M1 macrophages to shift to the M2 macrophage phenotype, thereby reducing the inflammatory cascade by decreasing RBC release of hemoglobin and thus endothelial dysfunction [32]. This chapter posits that while administration of aerosolized NO concurrently with O2 may modestly alleviate the inappropriate inflammatory cascade leading to endothelial dysfunction, a better delivery mechanism for NO may help systemic inflammatory damage caused by ARDS by increasing NO bioavailability. To accomplish this, we highlight the efficacy of nitric oxide releasing nanoparticles (NOnps) in a preclinical model of ARDS and demonstrate reduced hypoxemia and reduced neutrophil mediated inflammation [4].

Engineering the Microvasculature – Implications. The microvasculature is highly dynamic and diverse and can be leveraged for broad therapies for a variety of diseases with underlying microvascular dysfunction. Engineering specific interventions, whether mechanical or molecular, to specifically target microvascular dysfunction of several etiologies provides a novel means for drug and device design. In hemorrhagic shock, this thesis utilizes a mechanical intervention, namely a negative pressure window chamber, and leveraged transluminal hydrostatic pressure gradients in the microcirculation to transientyl increase perfusion without the need for volume resuscitation. In neoplasia, the RBCs themselves were used as delivery vehicle to both induce oxidative stress to reduce tumor viability and induce vaso-occlusion to direct flow through more efficient microvessels, promoting chemo sensitization. Lastly, NOnps were used to alleviate the inflammatory response in ARDS to reduce endothelial dysfunction by improving nitric oxide

6

bioavailability. Systemic microcirculatory dysfunction in ARDS was also improved with NOnps, despite treatment being applied directly to the lung. These interventions were conceived with an intimate understanding of the microcirculation and engineering principles. While still immature for clinical use, this approach to engineering interventions by targeting the microcirculation has broad potential for clinical application and potentially introduce a new class of specific microcirculatory-directed therapies.

Chapter 1

Application of negative tissue interstitial pressure improves functional capillary density after hemorrhagic shock in the absence of volume resuscitation

Abstract: Microvascular fluid exchange is primarily dependent on Starling forces and both the active and passive myogenic response of arterioles and post-capillary venules. Arterioles are classically considered resistance vessels, while venules are considered capacitance vessels with high distensibility and low tonic sympathetic stimulation at rest. However, few studies have investigated the effects of modulating interstitial hydrostatic pressure, particularly in the context of hemorrhagic shock. The objective of this study was to investigate the mechanics of arterioles and functional capillary density (FCD) during application of negative tissue interstitial pressure after 40% total blood volume hemorrhagic shock. In this study, we characterized systemic and microcirculatory hemodynamic parameters, including FCD, in hamsters instrumented with a dorsal window chamber and a custom-designed negative pressure application device via intravital microscopy. In large arterioles, application of negative pressure after hemorrhagic shock resulted in a $13\pm11\%$ decrease in flow compared with only a $7\pm9\%$ decrease in flow after hemorrhagic shock alone after 90 minutes. In post-capillary venules, however, application of negative pressure after hemorrhagic shock resulted in a $31\pm4\%$ decrease in flow compared with only an $8\pm5\%$ decrease in flow after hemorrhagic shock alone after 90 minutes. Normalized FCD was observed to significantly improve after application of negative pressure after hemorrhagic shock (0.66 ± 0.02)

compared to hemorrhagic shock without application of negative pressure (0.50 ± 0.04). Our study demonstrates that application of negative pressure acutely improves FCD during hemorrhagic shock, though it does not normalize FCD. These results suggest that by increasing the hydrostatic pressure gradient between the microvasculature and interstitium, microvascular perfusion can be transiently restored in the absence of volume resuscitation. This study has significant clinical implications, particularly in negative pressure wound therapy, and offers an alternative mechanism to improve microvascular perfusion during hypovolemic shock.

Keywords: functional capillary density, microcirculation, negative pressure, Starling forces

1.1 Introduction

Severe hemorrhagic shock is a known cause of widespread organ failure even after correction of systemic hemodynamics with transfusion [14, 19]. Despite correction of systemic hemodynamics, microvascular perfusion often remains impaired [14, 19]. *In vivo*, microvascular fluid exchange is primarily dependent on Starling forces. Microvascular fluid flux is a function of capillary and interstitial hydrostatic and oncotic pressures. The volumetric filtration flux of fluid through the capillary wall per unit area, J_V/A, is described by the Starling equation, shown below,

$$J_V/A = L_P\left[(P_c - P_i) - \sigma\left(\pi_c - \pi_i\right)\right] \tag{1.1}$$

where P_c and P_i are the capillary and interstitial hydrostatic pressures, respectively, π_c and π_i are the capillary and interstitial oncotic pressures, respectively, L_P is the permeability of the capillary wall, and σ is Staverman's oncotic reflection coefficient [33, 34]. Under normal physiological conditions, oncotic pressure drives vascular resorption as the vascular hydrostatic pressure must be greater than the interstitial hydrostatic pressure to reduce vascular compression [35]. Recent evidence suggests that the endothelial glycocalyx, a complex layer of glycoproteins and proteoglycans, plays a larger role in microvascular fluid absorption and has led to a revision

of Starling's principles. The large porous structure of the glycocalyx creates a "protected region" proximal to the endothelial cell surface, which possesses a low oncotic pressure relative to the protein-rich glycocalyx, enhancing volumetric filtration [36]. Modifications to the glycocalyx in diabetes, shock, and atherosclerosis consequently have unexpected effects on the microvascular fluid flux that were previously underappreciated. In these cases, interstitial edema can form due to changes in hydrostatic pressure, as observed in pulmonary edema secondary to left ventricular failure [37], or an increase in vascular permeability and subsequent loss of the glycocalyx endothelial oncotic pressure gradient, as observed in acute respiratory distress syndrome (ARDS) [38, 37]. An understanding of the Starling forces can be leveraged to reverse interstitial edema. For instance, it has been shown that interstitial edema can be reversed by increasing plasma oncotic pressure [35]. However, few studies have investigated the effects of modulating interstitial hydrostatic pressure, particularly in the context of hemorrhagic shock.

In addition to Starling forces, microvascular fluid flux is dependent on both the active and passive myogenic properties of arterioles and post-capillary venules. Arterioles are classically considered resistance vessels, with tonic sympathetic stimulation predominantly determining resting wall tension [39, 40]. The active myogenic response is a calcium-dependent process and is triggered by increased wall tension or vascular stretch, generally secondary to vessel distension from increased hydrostatic pressure [41]. The passive elastic properties result from the connective tissue wall composition: elastin conferring elasticity and collagen conferring stiffness. Importantly, alterations in passive stiffness adversely affect pressure sensing and can inhibit the myogenic response, as observed in microvascular angiopathy secondary to diabetes and hypertension [42, 43]. Arteriolar tone also controls FCD and thus is responsible for modulating microvascular perfusion [44, 45]. The passive circumferential properties of venules are Hookean at any given level of sympathetic tone due to their thin walls [46, 47]. Few studies, however, have investigated the effects of changing tissue interstitial pressure on microvascular myogenic properties.

Methods to correct impaired perfusion during hemorrhage have centered around altering blood rheology, modulating Starling forces, and by pharmacologically increasing sympathetic stimulation of the microvasculature. The viscosity of blood in circulation has shown to be an important factor in resuscitation from hemorrhagic shock. Many studies have established that loss of blood viscosity from hemodilution and transfusion result in microvascular endothelial injury, tissue damage, and death [14, 19, 48]. As a result, it has been hypothesized that supplemental transfusion with high viscosity plasma expanders may improve perfusion. Much work has demonstrated that high viscosity plasma expanders used concomitantly with blood transfusion improve microvascular perfusion and FCD during hemorrhagic shock [14, 19, 48]. However, these methods may result in extreme hemodilution, which results in decreased O_2 carrying capacity and impaired FCD [14, 19, 48]. We hypothesize that application of a negative tissue interstitial pressure may serve to improve microvascular perfusion during hemorrhagic shock to compensate for the loss in hydrostatic pressure gradient, and as such could act as an alternative to fluid resuscitation. Therefore, the objective of this study was to investigate the mechanics of dynamics in arterioles and FCD during application of negative tissue interstitial pressure after hemorrhagic shock.

1.2 Materials and Methods

1.2.1 Animal Preparation

Male Syrian Golden hamsters weighing 55 to 70 g (Charles River Laboratories, Boston, MA) were fitted with a dorsal skinfold window chamber model. Care and handling of hamsters abided by the NIH Guide for the Care and Use of Laboratory Animals. Approval of the study was given by the University of California San Diego Institutional Animal Care and Use Committee. The window chamber preparation is a well-established model of microvascular blood flow in intact tissue that can be studied without anesthesia [49]. Tissues studied in this model include

skeletal muscle and subcutaneous connective tissue, described in detail elsewhere [49]. Chamber implantation was performed under anesthesia (200 mg/kg ketamine and 10 mg/ kg xylazine IP). Briefly, the chamber consists of 2 titanium frames with a 15-mm-diameter circulation observation window; 1 frame of the chamber was placed in direct contact with animal skin. Sutures were placed to lift the dorsal skin away from the animal. The skinfold was removed following the out- line of the window until only a thin monolayer of muscle and skin remained. A cover glass was placed on the exposed tissue and held in place by the other frame under a drop of saline. A minimum of 48 hours was allowed for recovery prior to catheterization. Chambers with signs of edema, bleeding, or neovascularization were not used. Animals were re-anesthetized as described, and carotid (arterial) and jugular (venous) catheters were implanted and exteriorized at the dorsal side of the neck, where they were attached to the chamber frame for easy access. The animals were then allowed another day for recovery prior to experimentation. Experimentation was performed in the awake, unanesthetized state.

1.2.2   Inclusion Criteria

Inclusion criteria included the following: (1) systemic parameters within reference range at baseline (heart rate (HR) > 340 beats per minute, mean arterial pressure (MAP) > 80 mmHg and < 130 mmHg, systemic hematocrit (Hct) > 45%, PaO_2 > 50 mmHg), and (2) no signs of edema, bleeding, or unusual neovascularization of tissue in the chamber under 20x magnification. Note that PaO_2 > 50 mmHg is considered normal for hamsters; however, microvascular pO_2 distribution is similar to that of other rodents [18].

1.2.3   Negative tissue interstitial pressure application protocol

A 15-mm-diameter circular chamber was constructed from acrylic for application of negative tissue interstitial pressure. Device specifications are shown in Figure 1.1. Application of negative tissue interstitial pressure involved attachment of the device to the intact subcutaneous skin on the
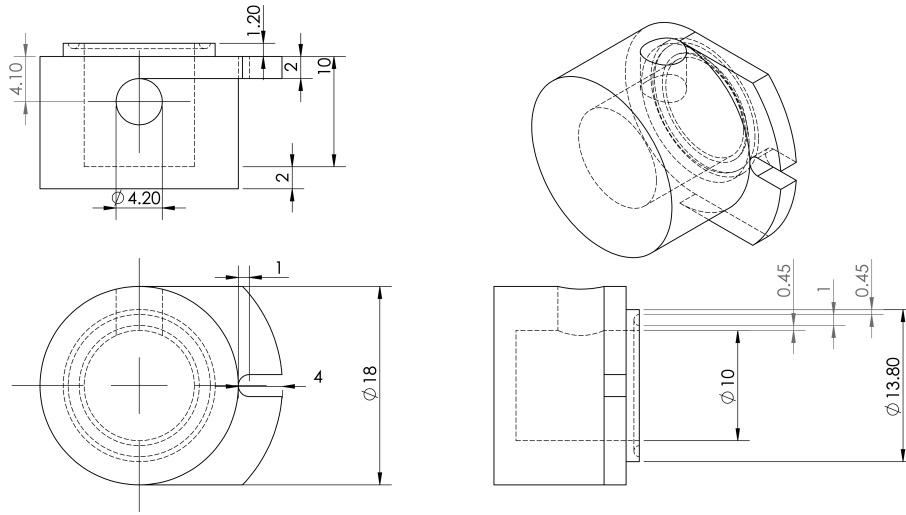
Figure 1.1: Schematic of Custom-designed Negative Pressure Chamber. A negative pressure chamber was designed using SolidWorks and constructed using acrylic in order to locally apply negative pressure to the hamster dorsal skin fold window chamber model.

back of the chamber. Briefly, a copious amount of high-grade silicon grease (Anchor Electronics, Santa Clara, CA) was applied to the 1.2 mm lip of the device with a wooden applicator and placed in direct contact with the subcutaneous skin and secured onto the chamber. To create a vacuum seal, a luer adapter was fixed to the port located on the side of the chamber and connected to a clear PVC 1/8-inch inner diameter tubing (Fisher Scientific, Waltham, MA). The tubing was secured to a 10-mL syringe and pressure transducer (MP150; Biopac Systems, Santa Barbara, CA) with a three-way luer adapter. Pressure was adjusted by modulating the volume of saline in the 10 mL syringe. The experimental setup is described in detail elsewhere [50]. For all experiments, a negative 4 mmHg interstitial pressure was applied either after baseline or 5 minutes after 40% hemorrhage, protocol detailed below. The degree of negative pressure applied was manually adjusted throughout the entire experiment to account for air leak.

1.2.4 Hemorrhage and negative pressure protocol

Acute hemorrhage was produced by withdrawal of 40% of the total animal blood volume (BV) via the carotid artery catheter within 5 minutes. BV was estimated as 7% of animal body
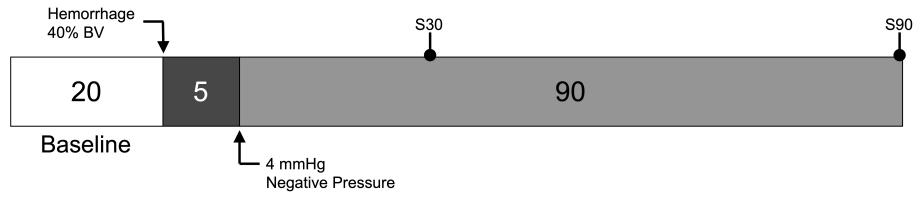
Figure 1.2: Experimental Timeline. Acute hemorrhage was produced by withdrawal of 40% of the total animal blood volume (BV) via the carotid artery catheter within 5 minutes. BV was estimated as 7% of animal body weight. The parameters analyzed were measured before hemorrhage induction (baseline), and 30 and 90 minutes after hemorrhage.

weight. The parameters analyzed were measured before hemorrhage induction (baseline), and 30 and 90 minutes after hemorrhage. A schematic timeline of the protocol is shown in Figure 1.2.

1.2.5   Systemic hemodynamic and blood gas parameter

Mean arterial pressure (MAP) and heart rate (HR) were con- tinuously recorded throughout the entire experiment (MP150; Biopac Systems, Santa Barbara, CA). Arterial blood was collected in heparinized capillary tubes and analyzed for PaO_2, $PaCO_2$, anion gap, and pH (Blood Chemistry Analyzer 248; Bayer, Norwood, MA). The Hct was measured from centrifuged arterial blood taken in heparinized capillary tubes. The Hb concentrations were measured spectrophotometrically using the B-Hemoglobin (HemoCue, Stockholm, Sweden) from a drop of arterial blood [51, 52].

1.2.6   Microvascular Experimental setup

The awake animals were placed in a restraint tube with a slit to accommodate the window chamber. The restraint tube was then fixed to a microscopic stage of a transillumination intravital microscope (BX51WI; Olympus, New Hyde Park, NY). Measurements were performed after 20 minutes to allow for adjustment to the tube environment with a 40× (LUMPFL-WIR, numerical aperture of 0.8; Olympus) water immersion objective.

1.2.7 Microhemodynamics

Detailed mappings of the chamber vasculature were acquired at baseline to ensure the same vessels were followed throughout the experiment. Arteriolar and venular blood flow velocities were measured online using the photodiode cross-correlation method (Photo-Diode/Velocity; Vista Electronics, San Diego, CA) [53]. The measured centerline velocity (V) was normalized to baseline blood vessel measurements to obtain the normalized mean RBC velocity. A video image shearing method was used to measure blood vessel diameter (D), which was normalized to the baseline recording. Blood flow (Q) was computed using Poiseuille's law, $Q = \pi \times V \times (D/2)^2$ and normalized to the flow computed at baseline.

1.2.8 Functional capillary density

Functional capillaries were defined as capillary segments with transit of at least a single RBC in a 15-second interval. FCD was assessed in 10 successive microscopic fields, totaling a region of 0.46 mm^2. The fields were chosen at baseline by a distinctive anatomical (i.e., large bifurcation) or structural landmark. Observation of the fields was performed systematically by adjusting the microscope field of view by one field width in 10 successive steps, each 240 μm in length relative to the tissue. Each field had between 2 and 10 capillary segments with RBC flow at baseline. FCD is measured in cm^{-1} and calculated by adding the length of capillaries that had RBC transit in the field of view and dividing over the area of the microscope field of view. The relative change in FCD from baseline after each intervention is indicative of microvascular tissue perfusion [54].

1.2.9 Statistical Analysis

All data are represented as mean $\pm$ SD. Data were compared using a two-way ANOVA, with row and column factors being time after treatment and group, respectively. When appropriate, post hoc analysis was performed with Holm–Sidak multiple comparisons test for parametric data.

Microhemodynamic data are presented as ratios relative to baseline to account for differences in vessel diameter. The same blood vessels and capillary fields were monitored throughout each experiment to allow for direct comparisons to baseline. Comparisons to baseline were via Student's t test. All statistical analyses were performed in GraphPad Prism 8.3 (GraphPad Software, San Diego, CA). Changes were considered significant if p values were < 0.05.

1.3   Results

A total of fifteen animals (n $=$ 15) were included in this study. Animals were randomly assigned to each experimental group based on application of negative pressure. These groups were (i) negative pressure during normovolemia, labeled Negative Pressure (no Hemorrhage), n $=$ 5; (ii) hypovolemia (40% BV hemorrhage) without application of negative pressure, labeled 40% Hemorrhage, n $=$ 5; and (iii) negative pressure during hypovolemia (40% BV hemorrhage), labeled Negative Pressure after 40% Hemorrhage, n $=$ 5. For each animal, between four and six arterioles and four and six venules were selected after application of systemic and vessel inclusion criteria. The parameters analyzed were measured before hemorrhage induction (baseline), and 30 and 90 minutes after hemorrhage. There were no significant differences in hematocrit, systemic, or microhemodynamic parameters at baseline among all animals in all groups.

1.3.1   Systemic Parameters

Systemic hemodynamic parameters are summarized in Figure 1.3. Briefly, there were no significant differences in heart rate between groups at 30 and 90 minutes, though the change in heart rate was significant with time ($p < 0.05$). Mean arterial pressure (MAP), hematocrit, and hemoglobin reflect changes expected from 40% BV hemorrhage.
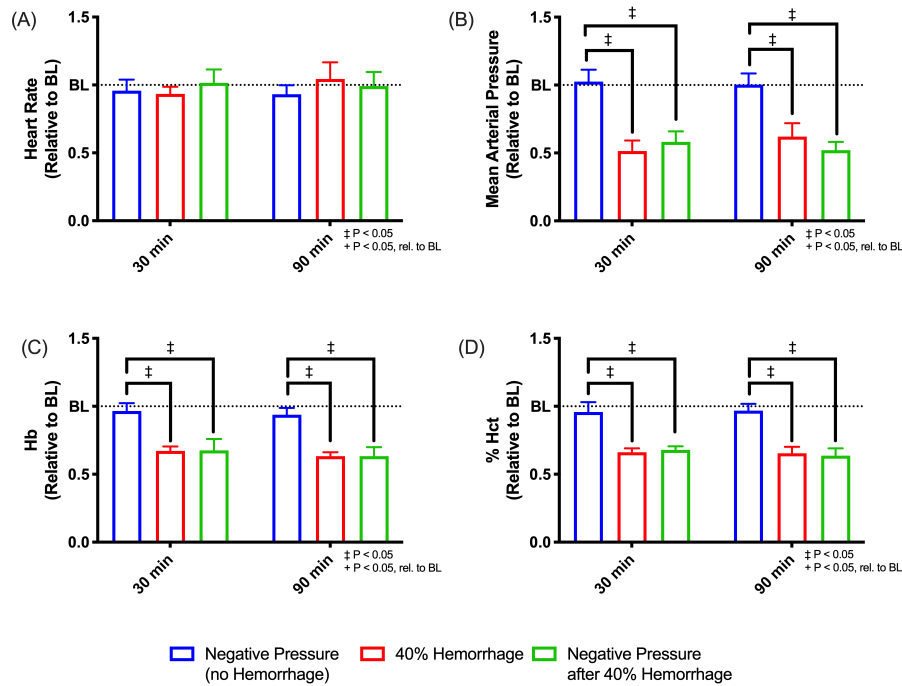
Figure 1.3: Systemic Hemodynamics. Systemic hemodynamic parameters were assessed at baseline, 30 minutes after intervention, and 90 minutes after intervention for all groups, (i) negative pressure during normovolemia, labeled Negative Pressure (no Hemorrhage), n = 5; (ii) hypovolemia (40% BV hemorrhage) without application of negative pressure, labeled 40% Hemorrhage, n = 5; and (iii) negative pressure during hypovolemia (40% BV hemorrhage), labeled Negative Pressure after 40% Hemorrhage, n = 5. Hemodynamics shown include the following: (a) heart rate, (b) mean arterial pressure, (c) hemoglobin (Hb) concentration (g/dL), and (d) % hematocrit (Hct). All results were normalized relative to measured results at baseline. Changes in MAP, Hb, and % Hct reflect the expected changes. +: $p < 0.05$ rel. to baseline. ‡:$p < 0.05$ between groups.

1.3.2 Microvascular Diamater

Arteriolar and venular diameters for all groups are summarized in Figure 1.4. Application of negative pressure after 40% hemorrhage significantly increased arteriolar diameter at 30 minutes ($p < 0.05$) compared to baseline. However, no significant changes in diameter were observed compared to baseline at 90 minutes in this group (Figure 1.4a). Subgroup analysis was performed based on arteriolar size. For arterioles <40 μm, a statistically significant increase ($p < 0.05$) in diameter was observed with 40% hemorrhage both with and without application of negative pressure at 30 minutes. Though, at 90 minutes, this significant increase in diameter
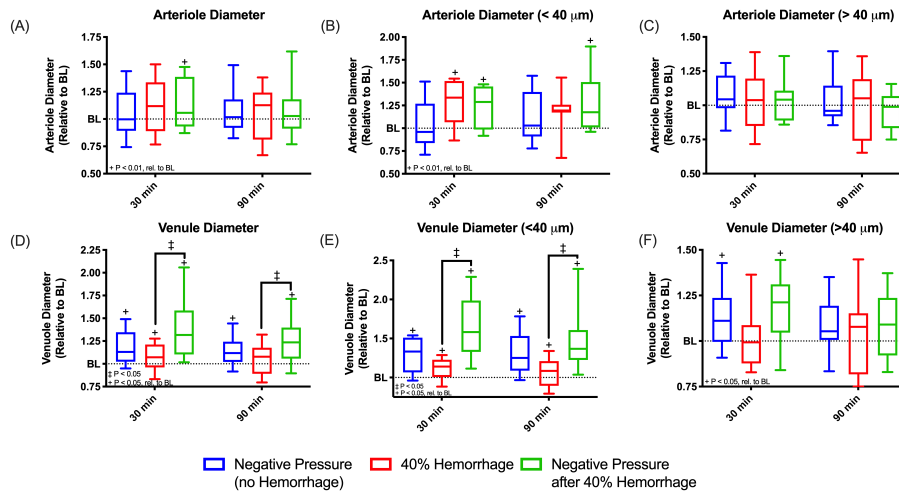
Figure 1.4: Arteriolar and Venular Diameter with Subgroup Analysis. Arteriolar and venular diameter was measured using an image shearing technique and assessed at baseline, 30 minutes after intervention, and 90 minutes after intervention for all groups, (i) negative pressure during normovolemia, labeled Negative Pressure (no Hemorrhage), n = 5; (ii) hypovolemia (40% BV hemorrhage) without application of negative pressure, labeled 40% Hemorrhage, n = 5; and (iii) negative pressure during hypovolemia (40% BV hemorrhage), labeled Negative Pressure after 40% Hemorrhage, n = 5. All values are normalized with respect to baseline. Subgroup analysis was performed based on vessel size. Plots shown are as follows: (a) arteriolar diameter (All), (b) arteriole diameter ($< 40\,\mu$m), (c) arteriole diameter ($> 40\,\mu$m), (d) venular diameter (All), (e) venular diameter ($< 40\,\mu$m), and (f) venular diameter ($> 40\,\mu$m). +: p ¡ 0.05 rel. to baseline. ‡:p < 0.05 between groups.

was sustained only with application of negative pressure with 40% hemorrhage (Figure 1.4b). For larger arterioles $>40\,\mu$m, no significant differences were observed relative to baseline and between groups for all times assessed (Figure 1.4c).

There was a significant increase in venular diameter (p < 0.05) relative to baseline for all groups at 30 minutes. Similarly, at 90 minutes, venular diameter was significantly increased relative to baseline with application of negative pressure regardless of volume status (Figure 1.4d). Venular diameter was significantly larger with application of negative pressure after 40% hemorrhage compared to hemorrhage at all time points (Figure 1.4d). Similar results were observed when analyzing only venules $< 40\,\mu$m (Figure 1.4e). For venules $>40\,\mu$m, a significant increase in diameter was observed relative to baseline with application of negative pressure regardless of volume status at 30 minutes (Figure 1.4f).

1.3.3 Microvascular Velocity

Arteriolar and venular velocities in all groups are summarized in Figure 1.5. A significant decrease in velocity ($p < 0.05$) was observed in arterioles after 40% hemorrhage regardless of negative pressure application relative to baseline at all time points (Figure 1.5a). For arterioles < 40 μm , a statistically significant decrease ($p < 0.05$) in velocity was observed relative to baseline after 40% hemorrhage with application of negative pressure at 30 minutes. At 90 minutes, small (<40 μm) arteriolar velocity was decreased relative to baseline for all groups (Figure 1.5b). For arterioles > 40 μm, velocity was significantly decreased with 40% hemorrhage regardless of application of negative pressure at all time points (Figure 1.5c).

Venular velocity was significantly decreased relative to baseline after 40% hemorrhage regardless of application of negative pressure at all time points. Additionally, after 90 minutes venular velocity was significantly decreased after application of negative pressure after 40% hemorrhage compared to hemorrhage alone (Figure 1.5d). Subgroup analysis was performed based on venular size. Briefly, results were similar to those described above for venules < 40 μm;however, a significant decrease in velocity was observed relative to baseline with application of negative pressure during normovolemia at 90 minutes, though not in 40% hemorrhage alone (Figure 1.5e). In venules >40 μm, a statistically significant decrease in venular velocity was observed relative to baseline only in the Negative Pressure (no Hemorrhage) group at 30 minutes, though not at 90 minutes. Surprisingly, application of negative pressure after 40% hemorrhage resulted in a significant decrease in venular velocity relative to baseline (Figure 1.5f).

1.3.4 Microvascular Flow

Flow was calculated for both arterioles and venules from Poiseuille's equation with the measured diameters and velocities described above (Figure 1.6). No statistically significant differences in arteriolar flow relative to baseline or between groups were observed (Figure 1.6a). Subgroup analysis revealed similar results for arteriolar flow for small arterioles <40 μm (Figure
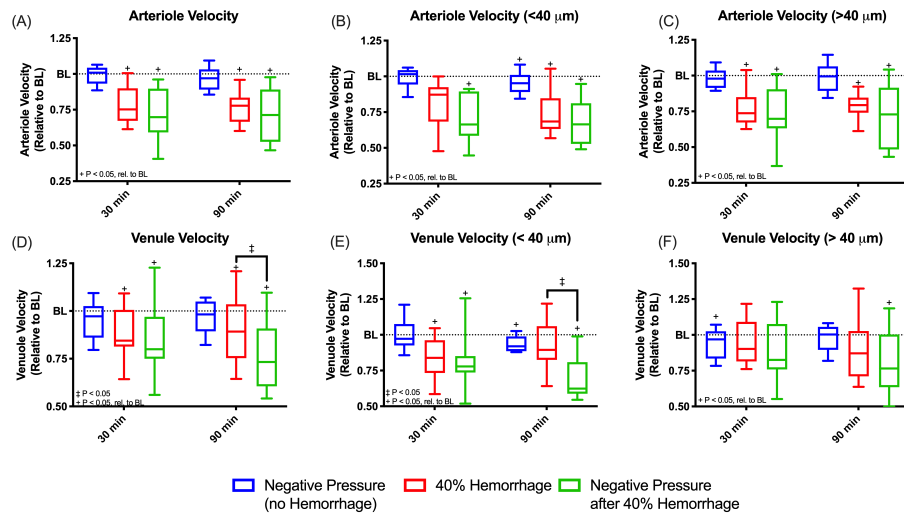
Figure 1.5: Arteriolar and Venular Velocity with Subgroup Analysis.Arteriolar and venular velocities were measured using intravital microscopy and assessed at baseline, 30 minutes after intervention, and 90 minutes after intervention for all groups, (i) negative pressure during normovolemia, labeled Negative Pressure (no Hemorrhage), n = 5; (ii) hypovolemia (40% BV hemorrhage) without application of negative pressure, labeled 40% Hemorrhage, n = 5; and (iii) negative pressure during hypovolemia (40% BV hemorrhage), labeled Negative Pressure after 40% Hemorrhage, n =5. All values are normalized with respect to baseline. Subgroup analysis was performed based on vessel size. Plots shown are as follows: (a) arteriolar velocity (All), (b) arteriole velocity ($< 40\,\mu$m), (c) arteriole velocity ($> 40\,\mu$m), (d) venular velocity (All), (e) venular velocity ($< 40\,\mu$m), and (f) venular velocity ($> 40\,\mu$m). +: $p < 0.05$ rel. to baseline. ‡:$p < 0.05$ between groups.

1.6b). In large arterioles ($>40\,\mu$m), a statistically significant decrease in flow relative to baseline was observed in the Negative Pressure after 40% Hemorrhage group at all time points (Figure 1.6c). Furthermore, arteriolar flow was significantly decreased with application of negative pressure with the 40% hemorrhage compared to hemorrhage alone.

A significant increase in venular flow was observed with application of negative pressure with 40% hemorrhage compared to hemorrhage alone at all time points (Figure 1.6d). Subgroup analysis revealed similar results for arteriolar flow for small venules $<40\,\mu$m (Figure 1.6e). In large venules ($>40\,\mu$m), a statistically significant increase in flow was observed relative to baseline with application of negative pressure regardless of volume status (Figure 1.6f). No statistically significant changes between groups were observed for these venules.

20
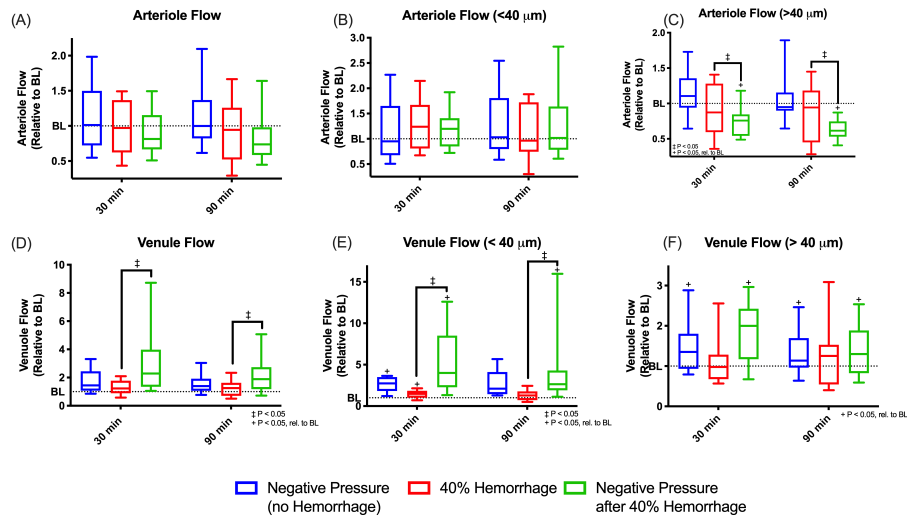
Figure 1.6: Arteriolar and Venular Flow with Subgroup Analysis. Arteriolar flow and venular flow were calculated using Poiseuille's law and assessed at baseline, 30 minutes after intervention, and 90 minutes after intervention for all groups, (i) negative pressure during normovolemia, labeled Negative Pressure (no Hemorrhage), n = 5; (ii) hypovolemia (40% BV hemorrhage) without application of negative pressure, labeled 40% Hemorrhage, n = 5; and (iii) negative pressure during hypovolemia (40% BV hemorrhage), labeled Negative Pressure after 40% Hemorrhage, n = 5. All values are normalized with respect to baseline. Subgroup analysis was performed based on vessel size. Plots shown are as follows: (a) arteriolar flow (All), (b) arteriole flow ($< 40\ \mu$m), (c) arteriole flow ($> 40\ \mu$m), (d) venular flow (All), (e) venular flow ($< 40\ \mu$m), and (f) venular flow ($> 40\ \mu$m). +: $p < 0.05$ rel. to baseline. ‡: $p < 0.05$ between groups.

1.3.5 Functional Capillary Density

Functional capillary density (FCD) for all groups is shown in Figure 1.7. A statistically significant increase in FCD was observed relative to baseline with application of negative pressure. As expected, a statistically significant decrease in FCD was observed relative to baseline after 40% hemorrhage regardless of volume status. Surprisingly, at 30 minutes, FCD was significantly higher with application of negative pressure after 40% hemorrhage compared to hemorrhage alone ($p < 0.05$). This difference was not sustained 90 minutes after 40% hemorrhage.

Functional Capillary Density (FCD)
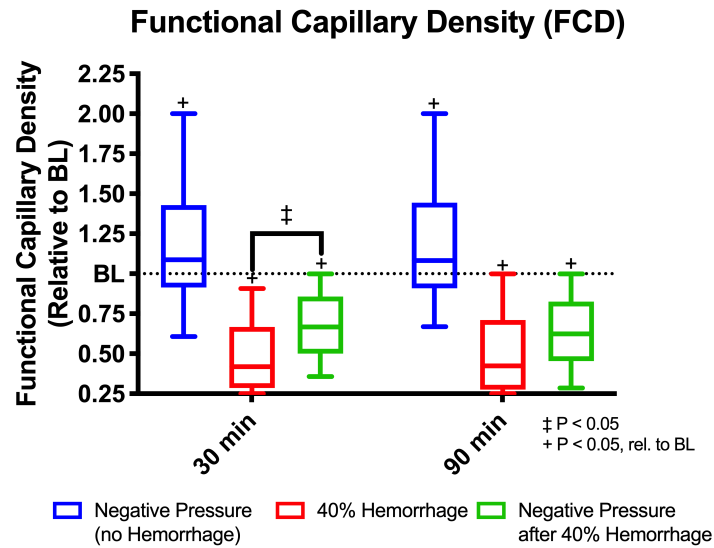
Figure 1.7: Functional Capillary Density.Functional capillary density was assessed using intravital microscopy at baseline, 30 minutes after intervention, and 90 minutes after intervention for all groups, (i) negative pressure during normovolemia, labeled Negative Pressure (no Hemorrhage), n = 5; (ii) hypovolemia (40% BV hemorrhage) without application of negative pressure, labeled 40% Hemorrhage, n = 5; and (iii) negative pressure during hypovolemia (40% BV hemorrhage), labeled Negative Pressure after 40% Hemorrhage, n = 5. +: p < 0.05 rel. to baseline. ‡:p < 0.05 between groups.

1.4 Discussion

This study evaluates the effects of applied negative tissue interstitial pressure on microvascular perfusion both during normovolemia and after hemorrhagic shock. The principle findings of this study are as follows: (i) In normovolemia, application of constant negative tissue interstitial pressure acutely increases FCD and venular outflow, indicating increased microvascular perfusion and intramural capillary pressure, respectively; (ii) in hemorrhagic shock, application of negative pressure acutely improves FCD, though does not normalize it; and (iii) in both normovolemia and hypovolemia, application of negative tissue interstitial pressure increases mean capillary perfusion pressure by increasing venular outflow while maintaining arteriolar inflow. These results suggest that by increasing the hydrostatic pressure gradient between the microvasculature and interstitium, microvascular perfusion can be transiently restored in the absence of volume resuscitation.

Importantly, these changes were not sustained in our studies, and alternative interventions may be required for chronic management of hypovolemic shock. Multiple interventions, namely high viscosity plasma expanders, have demonstrated improvement in microvascular perfusion without packed red cell transfusion [14, 55]. However, few studies have investigated transfusion-independent methodologies for restoration of microvascular perfusion in hemorrhagic shock. The findings from this study have significant clinical implications, particularly for reducing edema during surgical wound closure (i.e., negative pressure wound therapy) [56].

Application of negative pressure did little to mitigate the vascular response in smaller arteriole beds during hemorrhagic shock. Surprisingly, however, there was a significant decrease in flow in larger arterioles that feed these smaller microvascular networks. During hemorrhagic shock, there is a systemic decrease in MAP and microvascular wall shear stress, resulting in activation of the carotid body and local endothelin-mediated vasoconstriction secondary to transient hypoxia, respectively. A catecholamine surge from carotid body activation results in sympathetic stimulation of vascular α_1 adrenergic receptors resulting in systemic vasoconstriction. However, it is well known that variability in perfusion pressure and microvascular shear stress results in a heterogeneous myogenic response across any given microvascular network [57, 48, 58]. Changes in vessel diameter and flow therefore depend on the selection of the tissue analyzed and specific vessels measured. In our study, we observed a significant increase in the diameter of small arterioles during hemorrhagic shock in response to decreased perfusion pressure to maintain microvascular flow; this was limited to smaller arterioles as the mechanical properties of larger arterioles limit their maximum diameter [42, 40, 59].

The objective of myogenic response is to maintain constant circumferential, or hoop, stress during changes in vascular hydrostatic pressure. This response is responsible for limited changes in flow during hypovolemic shock [60, 61, 62, 63]. In our study, application of negative pressure during normovolemia had few effects on arteriolar flow. Surprisingly, application of negative pressure after hemorrhagic shock exacerbated the decrease in arteriolar flow. In this case, the

increase in transmural pressure is likely due to the decrease in interstitial pressure being greater than the decrease in capillary pressure.

As discussed, application of constant negative tissue in- terstitial pressure acutely increases venular outflow both during normovolemia and hypovolemia in vessels $<40\,\mu$m. These changes are due to the increased diameter of venules and are reflective of their passive mechanical properties.These changes are likely responsible for the transient increase in FCD with application of negative pressure during normovolemia, as FCD is linearly proportional to capillary transmural pressure [14]. Furthermore, the increase in capillary transmural pressure in response to negative pressure was significant enough to improve FCD transiently after hemorrhage, though not entirely corrective.

FCD and capillary inflow are grossly dependent on two factors, precapillary microvascular resistance and pericyte activity at the capillary orifice [44, 45]. Both these factors are responsible for adjusting capillary transmural pressure, which is linearly proportional to perfusion [14, 64]. Surprisingly, despite the decrease in precapillary flow in our results, we observed an increase in FCD. These data suggest that altering tissue hydrostatic pressure and thus Starling Forces alters the function of pericytes, the other component responsible for maintaining FCD. Future studies should aim to investigate the specific molecular response to negative tissue interstitial pressure in pericytes.

The clinical relevance of exogenous application of negative tissue interstitial pressure has primarily been limited to negative pressure wound therapy (NPWT) during surgical wound closure in orthopedic surgery and diabetes [56, 65, 66, 67]. However, in these situations, the objective of NPWT is to decrease interstitial edema to allow for more effective wound remodeling. Studies to assess the effects of NPWT on local microvascular perfusion and oxygenation have been limited, though results have been conflicting [68, 69, 70, 71]. Sogorski et al. demonstrated a significant increase in oxygen saturation and red cell velocity in the microcirculation [71]. However, at low magnitudes of negative pressure in pigs, Borgquist et al. demonstrated a significant decrease in

vascular blood flow, consistent with the arteriolar findings observed in our studies [68]. Most studies, however, assessed total tissue perfusion and did not assess differences in arteriolar and venous flow and capillary perfusion. Furthermore, these studies investigated pressures in the range of -100 mmHg, in which vascular compression is a significant factor. Surprisingly, molecular studies have demonstrated accelerated microvessel maturation and increased pericyte recruitment with application of negative pressure by upregulation of angiogenin 1, tyrosine kinase receptor-2, a-smooth muscle actin, and collagen type IV [69]. Future studies are needed to further elucidate the mechanisms of pericyte function with exogenous negative pressure, especially in the context of hemorrhagic shock.

Our study has several limitations. Only animals that survived the shock protocol were included in the analysis. Kerger et al. demonstrated that arteriolar flow, vasomotion, and FCD are significantly different in animals that survived hemorrhagic shock compared to those that do not [57]. Future studies are required to assess the effect of negative pressure on survival in this protocol. Microvascular flow and FCD are dependent on vessel selection, which contributes to the high variability observed. Due to technical limitations, capillary transmural pressure was not directly measured, and hypotheses about its relevance for the results observed in this study must be considered with caution. Furthermore, the tissue interstitial pressure was not directly measured in this study, so it is unknown whether application was homogeneous within the entire chamber field of view, which may alter observed microvascular hemodynamics.

1.5   Conclusion

In summary, this study evaluates the effects of application negative tissue interstitial pressure on microvascular perfusion both during normovolemia and after hemorrhagic shock. Our results demonstrate that application of negative pressure acutely improves FCD after hemorrhagic shock, though it does not normalize it. These results suggest that by increas- ing the hydrostatic pressure gradient between the microvasculature and interstitium, microvascular perfusion can be transiently

restored in the absence of volume resuscitation. The physiology from this study has significant clinical implications, particularly in NPWT and offers an alternative mechanism to improve microvascular perfusion during hypovolemic shock. Future studies are required to assess the role of pericyte function and calcium transience after application of negative tissue interstitial pressure in these situations.

Chapter 1, in full, contains material as it appears in Application of negative tissue interstitial pressure improves functional capillary density after hemorrhagic shock in the absence of volume resuscitation. Jani, V. P., Jani, V. P., Munoz, C. J., Govender, K., Williams, A. T., and Cabrales, P. Physiological reports 9.5 (2021): e14783. The thesis author was the primary investigator and author of this paper.

Chapter 2

RRx-001 Increases Erythrocyte Preferential Adhesion to the Tumor Vasculature

Abstract: Red blood cells (RBCs) serve a variety of functions beyond mere oxygen transport both in health and pathology. Notably, RRx-001, a minimally toxic pleiotropic anticancer agent with macrophage activating and vascular normalization properties currently in Phase III trials, induces modification to RBCs which could promote vascular adhesion similar to sickle cells. This study assessed whether RBCs exposed to RRx-001 adhere to the tumor microvasculature and whether this adhesion alters tumor viability. We next investigated the biomechanics of RBC adhesion in the context of local inflammatory cytokines after treatment with RRx-001 as a potential mechanism for preferential tumor aggregation. Human HEP-G2 and HT-29 tumor cells were subcutaneously implanted into nu/nu mice and were infused with RRx-001-treated and Technetium-99m (^{99m} Tc)-labeled blood. RBC adhesion was quantified in an in vitro human umbilical vein endothelial cell (HUVEC) assay under both normoxic and hypoxic conditions with administration of either lipopolysaccharide (LPS) or Tumor necrosis alpha (TNFα) to mimic the known inflammation in the tumor microenvironment. One hour following administration of ^{99m} Tc labeled RBCs treated with 10 mg/kg RRx-001, we observed an approximate 2.0-fold and 1.5-fold increase in ^{99m} Tc-labeled RBCs compared to vehicle control in HEP-G2 and HT-29 tumor models, respectively. Furthermore, we observed an approximate 40% and 36% decrease in HEP-G2 and HT-29 tumor weight, respectively, following treatment with RRx-001. To quantify RBC adhesive potential, we determined τ_{50}, or the shear stress required for 50% disassociation of

RBCs from HUVECs. After administration of TNF-α under normoxia, τ_{50} was determined to be 4.5 dynes/cm2 (95% CI: 4.3-4.7 dynes/cm2) for RBCs treated with 10 μM RRx-001, which was significantly different (p < 0.05) from τ_{50} in the absence of treatment. Under hypoxic conditions, the difference of τ_{50} with (4.8 dynes/cm^2; 95% CI: 4.6-5.1 dynes/cm^2) and without (2.6 dynes/cm^2; 95% CI: 2.4-2.8 dynes/cm^2) 10 μM RRx-001 treatment was exacerbated (p = 0.05). In conclusion, we demonstrated that RBCs treated with RRx-001 preferentially aggregate in HEP-G2 and HT-29 tumors, likely due to interactions between RRx-001 and cysteine residues within RBCs. Furthermore, RRx-001 treated RBCs demonstrated increased adhesive potential to endothelial cells upon introduction of TNF-α and hypoxia suggesting that RRx-001 may induce preferential adhesion in the tumor but not in other tissues with endothelial dysfunction due to conditions prevalent in older cancer patients such as heart disease or diabetic vasculopathy.

Keywords: RRx-001; tumor microenvironment; RBC adhesion; shear stress

2.1   Introduction

RRx-001 is a minimally toxic pleiotropic anticancer agent with macrophage activating, CD47 downregulating and vascular normalizing properties currently under investigation in phase III clinical trials [72, 25]. A therapeutic on its own, RRx-001 is also a chemo- and radiosensitizer, augmenting traditional radiation and chemotherapeutics for solid tumor therapy primarily in the absence of systemic toxicities since the compound has not been associated with any dose limiting side effects in over 300 patients treated [73, 26]. Furthermore, the compound is a protective agent against chemotherapy and radiation-induced cytotoxicity in normal tissues, further highlighting its clinically utility. These seemingly counterintuitive effects of RRx-001 have been attributed to induction of nuclear factor erythroid 2–related factor 2 (Nrf2) in normal tissues, which is cytoprotective, while simultaneously inducing cytotoxicity in the tumor environment through downregulation of the anti-apoptotic Bcl2, downstream of Nrf2, as well as through CD47 antagonism, tumor associated macrophage (TAM) polarization, and vascular normalization [26].

The diverse functions and mechanisms surrounding RRx-001 cytotoxicity make it an attractive target for research. For instance, RRx-001 has been evaluated in melanoma [74], glial tissue (malignant glioblastoma) [74, 75], lung epithelium (small cell lung carcinoma) [25, 76], ovarian epithelium [26], and more recently, erythrocytes [72]. Interestingly, much like in sickle ane- mia, RRx-001 induces a dose dependent translocation of phospholipid phosphatidylserine (PS) and increased hemoglobin (Hb) oxidation in RBCs [27]. However, the mechanisms surrounding these effects remain underexplored.

Sickle cell red blood cells (sRBCs) are known to accumulate preferentially in the tumor vasculature, with the highest abundance observed at the interface between the tumor and normal tissue [77]. This phenomenon is likely due to the complex function of the tumor microenviron- ment, characterized by pockets of hypoxia, acidic conditions, reduced blood flow, and ischemia, all of which promote sickling and subsequently, sRBC aggregation [21]. The mechanism of sickling is well described and involves precipitation of sickle cell hemoglobin (Hb) within the microvasculature followed by subsequent formation of long Hb polymers, which further distort the biconcave erythrocyte structure, impair deformability, and increase PS expression [78]. This clinically manifests as vaso-occlusive crises, which continue to be a problem for clinical man- agement of sickle cell disease [79]. However, under normal physiologic conditions, sickling is an uncommon phenomenon in the absence of external stressors (e.g., infection induced acute chest syndrome) as sickling time is less than normal RBC capillary transit time. Importantly, the acidic and hypoxic tumor microenvironment, along with increased transit time secondary to increase vascular tortuosity and decreased blood flow provide sufficient stress to induce sickling, as shown by blood oxygen dependent imaging (BOLD) [27]. These data all demonstrate that the unique conditions and stressors imposed by the tumor microenvironment provide the necessary conditions for sickling and thus RBC aggregation.

As described, RRx-001 can induce increased externalization of PS, as is observed in sickle cell disease, which is thought to be due to increased Hb oxidation [27, 80]. The mechanism of

29

RRx-001 induced Hb oxidation involves increased nitric oxide production with subsequent (1) covalent binding of RRx-001 to the cysteine residue on the beta chain of hemoglobin, which under hypoxic conditions, increases conversion of nitrate to nitric oxide, and (2) RRx-001 dependent reaction with glutathione (GSH) and other thiols, which releases nitric oxide and other NOx variants [81, 82, 83]. When RRx-001 binds to Hb or reacts with GSH, nitro groups are lost, resulting in direct production of NO variants, all of which may induce NO mediated pathways. RRx-001 depletion of GSH and other antioxidant cysteine residues further contribute to oxidative stress. Oxidative injury can also result from formation of RRx-001-GSH adduct intermediaries, which further depletes GSH. Under hypoxic conditions, RRx-001 functionalized Hb has also been observed to produce more nitric oxide under hypoxic conditions. These mechanisms explain RRx-001's ability to increase denaturation and precipitation of hemoglobin. Thus, RRx-001 mediates oxidative injury in erythrocytes by increased production of nitric oxide and NO derived compounds, which result in increased reactive oxygen species and increased translocation of phospholipid phosphatidylserine in RBCs. The tumor microenvironment can also upregulate expression of the phospholipid phosphatidylserine receptor from hypoxia, increased inflammatory cytokines, and increased free heme. Together these data imply that RRx-001-modified RBCs may interact in unique ways with the tumor, which can be exploited for therapeutic potential [22].

This study exploits the observation that RRx-001 increases RBC membrane PS, while the tumor microvascular endothelium increases phospholipid phosphatidylserine receptor (PSR) to explore the effects of RRx-001 on RBCs within the tumor microenvironment. To this end, we assessed whether RBCs exposed to RRx-001 adhere to the tumor microvasculature and whether this adhesion alters tumor viability. We next investigated the biomechanics of RBC adhesion in the context of local inflammatory cytokines after treatment with RRx-001 as a potential mechanism for preferential tumor aggregation. We observed that RRx-001 treated RBCs preferentially aggregate in two known human cell line derived tumor models. Furthermore, we observed that RRx-001 treated RBCs demonstrated increased adhesive potential to endothelial cells upon introduction of

TNF-α and hypoxia, both of which increase endothelial PSR expression, suggesting that that the compound may induce preferential adhesion in the tumor.

2.2   Materials and Methods

2.2.1   RRx-001 RBC Treatment

Fresh blood was collected from C57BL/6J mice, weighing 20–24 g into syringes containing Anticoagulant Citrate Dextrose (ACD). For all animals in this study, the NIH Guide for the Care and Use of Laboratory Animals was followed. The study protocol was approved by the local animal care committee. Briefly, plasma and erythrocyte isolation were achieved via centrifugation (2000 rpm, 5 min), and the buffy coat was discarded. Plasma and packed RBCs were fixed. RRx-001 was mixed with blood to achieve concentrations equivalent to dosing mice with 1, 2, 5, 10, and 15 mg/kg. Blood mixtures were incubated with Tin (II) chloride ($SnCl_2$) at 1 mg/mL for 10 min. After incubation, 1 mCi 99mTc was added to this mixture, and the mixture was then incubated for 10 min. The sample mixture was then centrifuged (2500 rpm, 5 min), and the plasma and packed RBCs were separated. Aliquots of the plasma (P) and RBCs were precipitated with trichloroacetic acid (5%) and were then centrifuged (1500 rpm, 5 min) to isolate the soluble (SF) and insoluble (IF) fractions of the plasma and RBCs. Radioactivity of P, RBCs, SF-plasma, IF-plasma,SF-RBCs, and IF-RBCs were determined in a well counter, and the percentage of ^{99m}Tc incorporated ($\%^{99m}$Tc) was calculated.

2.2.2   Red Cell Treatment

Blood was collected from healthy volunteers into heparinized syringes and transferred into small tubes with CPD for a final anticoagulant to a blood ratio of approximately 1:7. Blood was centrifuged, and the buffy coat was discarded. RBCs were used fresh within 24 h of collection.

2.2.3 Human Endothelial Culture and Activation

Human umbilical vein endothelial cells (HUVECs) were purchased from the American Type Culture Collection (Manassas, VA abbrev, USA, Umbilical Vein Endothelial Cells; Normal). For adhesion experiments, HUVECs were cultured in gelatin-coated sterile glass coverslips and cultured at 37 $^\circ$ C at 5% CO_2 until confluent in Vascular Cell Basal media supplemented with 10% fetal calf serum (FCS) (Gibco, Life Technologies, Waltham, MA, USA), and 1% (100 μg/mL) penicillin/(100 μg/mL) streptomycin (Gibco, Life Technolo- gies). Prior to the RBC adhesion experiment, HUVECs monolayers were incubated with endotoxin (Lipopolysaccharides from Escherichia coli O111:B4 at 200 ng/mL; Sigma Aldrich, St Louis, MO, USA) or TNF-α (10 ng/mL) in culture media at 37 $^\circ$ C for 8 h.

2.2.4 RBC Adhesion Study

RBC adhesion to activated HUVECs was determined under continuous laminar flow of untreated RBCs (RBCs) or RBCs incubated with RRx-001 at (5 μM) (RRx-001-RBCs). Cells were diluted to a 2% hematocrit in 5% human serum albumin (Albuminar, Armour Pharmaceutical, Kanakee, IL, USA) solution in PBS. Confluent HUVEC layers were incubated with cells for 30 min before perfusion. After incubation with RBCs, suspended cells were washed three times with PBS, then the monolayers were perfused at incremental shear stresses with RBC free media for 2 min. The number of adhered RBCs was quantified before and after each shear exposure in 10 randomly selected sites within 2 min under no shear conditions. Studies were performed under oxygenated and deoxygenated conditions. For hypoxic conditions, HUVECs cells were incubated at 37 $^\circ$ C in a modular chamber flushed with 1% O_2, 5% CO_2 and 94% N_2, and red cells suspension and the solutions used in the adhesion study were also deoxygenated with 100% N_2 solution.

2.2.5 Erythrocyte Receptor Expression after RRx-001 Treatment

Treated and untreated red blood cells suspension (200 μL, about 2×10^7 total RBCs) were incubated for 60 min at room temperature with 100 μL diluted anti-CD36 monoclonal antibody (EPR6573, ab133625), anti-CD71 monoclonal antibody (EPR20584, ab214039), or anti-CD47 monoclonal antibody (EPR21794, ab218810) at a concentration of 5 μg/mL (all antibodies from ABCAM, Cambridge, MA, USA). These preparations then were washed twice in PBS and incubated with secondary fluorescent antibody. In addition, another sample was incubated with Annexin V-FITC Apoptosis Staining at 10 μg/mL (ab273273, ABCAM). Positive quantification was completed by hemocytometer.

2.2.6 Tissues and Solid Tumor RBC Accumulation Experimental Models

A total of 24 6-week-old athymic mice (nu/nu) were entered into the study and implanted with 20 μL (1×10^6 cells) of tumor suspension (either HEP-G2 cells or HT-29 cells). For all animals in this study, the NIH Guide for the Care and Use of Laboratory Animals was followed. The study protocol was approved by the local animal care committee. Briefly the tumor suspension consisted of human HEP-G2 cells (liver carcinoma cells) and HT- 29 cells (colorectal adenocarcinoma cells), which were suspended in Dulbecco's Modified Eagle Medium (DMEM) at 1×10^5 cells/μL for subcutaneous implantation. Two weeks after implantation of the tumor suspension, blood from nu/nu mice was collected and treated with RRx-001, and then labeled with ^{99m} Tc. Two concentrations of RRx-001, 5 mg/kg and 10 mg/kg along with a vehicle control were used, with n = 4/tumor type/group. This mixture was administered to the mice. Mice were euthanized 1 h after administration. After euthanasia, the vital organs, and both tumors were quickly isolated, weighed, and counted. The percentage of dose to weight was then determined.

2.2.7 Red Cell Dependent Activity of RRx-001 in Solid Tumors

In a different set of mice (nu/nu) either HEP-G2 cells (n = 4) or HT-29 (n = 4) cells were implanted as described before. One week after tumor implantation, blood from nu/nu mice was collected and treated with RRx-001 (5 mg/kg) and infused via tail vein. In addition, two control groups were used for the study, in one, animals received RRx-001 (5 mg/kg) in PBS without RBCs, and the other was an untreated control. RRx-001 treatments were repeated every 72 h. Tumor size was measured over 2 weeks, and animal were euthanized at the end of the study.

2.2.8 Statistical Analysis

Results are presented as mean $\pm$ standard deviation. All statistical calculations and graphics were performed and generated with a commercially available software package (GraphPad Prism 9.1, San Diego, CA, USA). To test differences in tumor localization, a 2-way ANOVA with post hoc Holm Sidak multiple comparisons between vehicle and RRx-001 doses was used. All data assessing RBC adhesion were fit to a three-parameter inverse sigmoidal curve. Differences in total body ^{99m} Tc and fit parameters were assessed using a nonparametric Kruskal-Wallis test with post hoc Dunn's multiple comparisons. For all tests, $p < 0.05$ was accepted as statistically significant.

2.3 Results

2.3.1 RRx-001 Localizes to RBCs

To test whether RRx-001 localized to RBCs and preferentially associated with hemoglobin in vitro, we treated RBCs with increasing concentrations of RRx-001, which is known to associate with Hb by oxidation of mercapto residues [81], and ^{99m} Tc , which is known to bind to mercapto residues at the Hb beta subunit [84]. These results are summarized in Figure 2.1A. Briefly, as expected, increasing concentrations of RRx-001 resulted in a dose dependent decrease in RBC
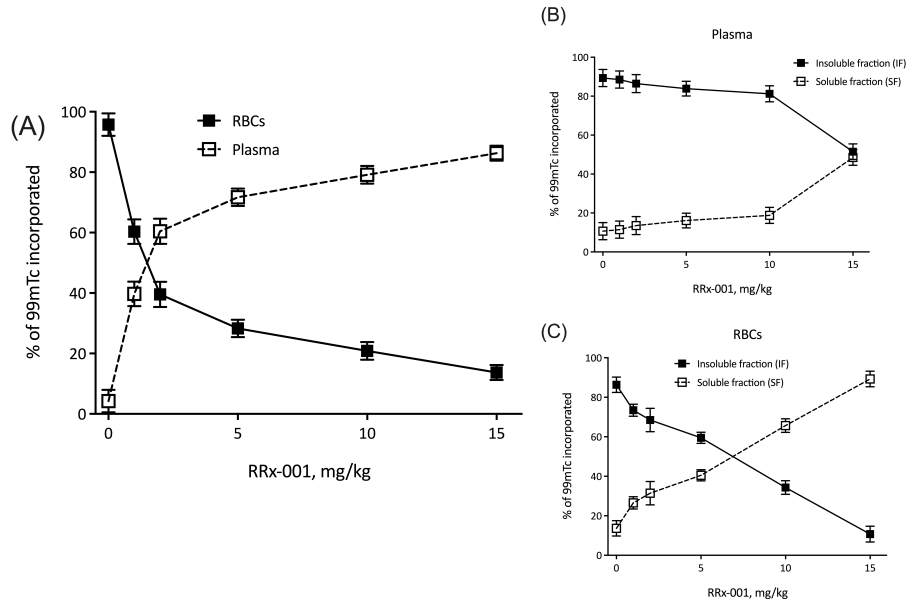
Figure 2.1: RRx-001 localizes to RBCs. Shown here are percent of ^{99m}Tc incorporated into **(A)** plasma and RBCs, **(B)** insoluble and soluble fractions of plasma, and **(C)** insoluble and soluble fractions of RBCs, all as a function of RRx-001 dose (mg/kg).

incorporated 99mTc, with $14 \pm 3\%$ ^{99m}Tc incorporated in RBCs at a dose of 15 mg/kg RRx-001. To determine whether RRx-001 predominantly associated with Hb, radioactivity of the soluble and insoluble fractions of both plasma (Figure 2.1B) and RBCs (Figure 2.1C) were probed, with the insoluble fraction of RBCs assumed to predominantly consist of Hb. In plasma, there was no change in the relative % ^{99m}Tc incorporated into insoluble and soluble protein fractions of plasma between 0 and 10 mg/kg RRx-001. At a dose of 15 mg/kg RRx-001, $52 \pm 4\%$ ^{99m}Tc was observed in the insoluble fraction,suggesting no preference of ^{99m}Tc labeling for either protein fraction at this concentration.However, in RBCs, there was an RRx-001 dose dependent decrease in % ^{99m}Tc incorporated in the insoluble protein fraction, with $11\pm4\%$ ^{99m}Tc incorporated in the insoluble fraction,suggesting that RRx-001 displaced radiolabeled ^{99m}Tc by associating with Hb.

2.3.2 RRx-001 Increases RBC Adhesion to the Endothelium

Given that RRx-001 treated RBCs preferentially localized to tumors in our animal models, we next sought to better understand the mechanism of this phenomenon. We hypothesized that RRx-001 increased RBC adhesive potential to the tumor endothelium. To characterize RBC adhesive potential after treatment of RRx-001, we utilized an in vitro HUVEC assay under hypoxic conditions with administration of either LPS or TNFα to mimic the hypoxia and cytokine mediated inflammation known to characterize the tumor microenvironment and induce endothelial phosphatidylserine receptor expression [22, 85, 86]. These results are summarized in Figure 2.2. To quantify RBC adhesion, adherent RBCs per mm^2 was plotted as a function of applied shear stress and fit to an inverse sigmoidal curve, and τ_{50}, or the shear stress required for 50% disassociation of RBCs from HUVECs, was calculated. Under LPS induced inflammation and normoxia, RRx-001 did not significantly change τ_{50}, 3.0 dynes/cm^2 and 2.6 dynes/cm^2 before and after 5 μM RRx-001 treatment, respectively (Figure 2.2A,F). This did not appreciably change under hypoxic conditions (Figure 2.2B,F). However, under TNFα induced inflammation, treatment with 10 μM RRx-001 induced a significant rightward shift in the curve (Figure 2.2C,D), with τ_{50} being significantly elevated ($p < 0.05$) after RRx-001 treatment, 3.1 dynes/cm^2 and 4.4 cm^2 before and after RRx-001 treatment, respectively (Figure 2.2F). Similar results were observed under hypoxic conditions (Figure 2.2D,F; $p < 0.05$). Importantly, no significant differences were observed in the number of adherent RBCs before application of shear stress (Figure 2.2E). Together, these results suggest that RRx-001 increased RBC adhesive potential to the endothelium under TNFα induced inflammation and hypoxia, as in the tumor microenvironment.

Membrane Receptor	Controls Mean $\pm$ SD	Before Mean $\pm$ SD	After Mean $\pm$ SD	p -Value
CD 36 (%)	0.5 ± 0.4	0.6 ± 0.3	2.5 ± 1.0*#	0.013
CD 71 (%)	0.9 ± 0.4	1.0 ± 0.8	4.2 ± 1.2*#	0.003
PS (%)	0.8 ± 0.4	1.2 ± 0.6	9.4 ± 1.4*#	0.002
CD 47 (%)	0.8 ± 0.3	0.9 ± 0.4	1.9 ± 0.8**	0.042

Table 2.1: Changes in Erythrocyte Receptor Expression after RRx-001 Treatment. $*$ p < 0.05 relative to controls. # p < 0.05 (paired t-test) relative to pre-treatment group.
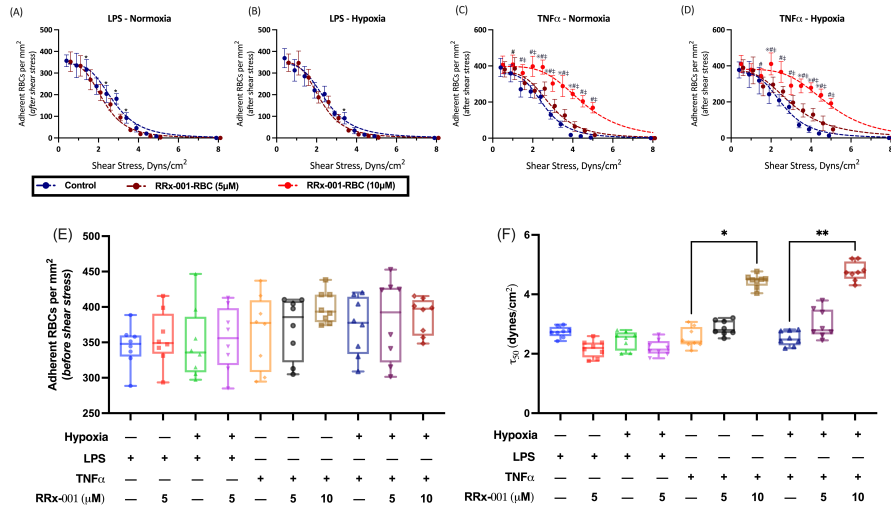
Figure 2.2: RRx-001 Induces Increased RBC Adhesion to the Endothelium. Adherent RBCs per mm^2 versus Shear Stress were fit to an inverse sigmodal curve and are shown for untreated and RRx-001 treated cells at 5 and 10 mg/kg under **(A)** LPS-induced inflammation and Normoxia, **(B)** LPS-induced inflammation and hypoxia, **(C)** TNFα induced inflammation and normoxia, **(D)** TNFα induced inflammation and hypoxia (* $p < 0.05$ Control vs. RRx-001 5 μM, # $p < 0.05$ Control vs. RRx-001 10 μM, ‡ $p < 0.05$ RRx-001 5 μM vs. RRx-001 10 μM). Fit parameters for inverse sigmoidal curves, namely **(E)** Adherent RBCs per mm^2 (before application of shear stress), and **(F)** τ_{50}, or the minimum shear stress for 50% disassociation of RBCs, are shown for the same parameters (* < 0.03, ** $p < 0.002$, for Holm-Sidak multiple comparisons).

2.3.3 RRx-001 Increases RBC Membrane Phospholipid Phosphatidylserine Expression

To further investigate the mechanism of increased RBC adhesion to the tumor microvascular endothelium, we measured the expression of several membrane receptors known to be affected by RRx-001, namely CD 36, CD 71, PS, and CD 47 (Table 2.1). We observed a significant increase in expression of all receptors (CD 36, CD 71, PS, and CD 47) measured. Specifically, there was a 6.8-fold increase in PS expression (p = 0.002) on the erythrocyte membrane. In the context of previous data showing an increase in PS receptor expression in the tumor microvascular endothelium [22], these data suggest that an increase in the PS and PS-receptor interaction after RBC treatment with RRx-001 is a viable mechanism for the observed increase in RBC adhesion.
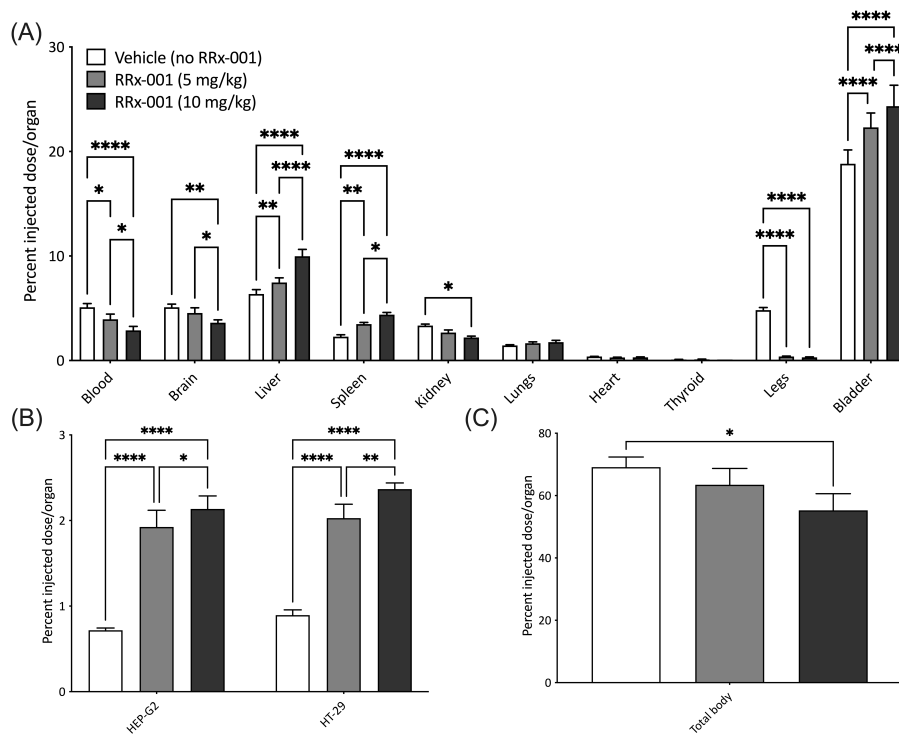
Figure 2.3: RRx-001 Treated RBCs Preferentially Localize to Solid Tumors. Shown here are percent injected dose/organ of ^{99m}Tc labeled blood for **(A)** blood, brain, liver, spleen, kidney, lungs, heart, thyroid, legs, and bladder **(B)** HEP-G2 and HT-29, and (C) total body ^{99m}Tc, for vehicle control (no RRx-001) and RRx-001 at concentrations of 5 and 10 mg/kg. (for Holm-Sidak multiple comparisons **(B)** or Dunn's multiple comparisons **(C)**).

2.3.4 RRx-001 Treated RBCs Preferentially Localize to Solid Tumors and Decrease Tumor Viability

To test whether RRx-001 treated RBCs preferentially localized to tumor cells, we utilized two experimental tumor models of human HEP-G2 (hepatocellular carcinoma) and HT-29 (colorectal carcinoma) cells implanted in nu/nu mice to account for the T cell tumor response. Both models were infused with RRx-001 treated- and ^{99m}Tc labeled-blood; results are summarized in Figure 2.3. The organ distribution of RRx-001 and vehicle in all experiments is summarized in Figure 3A. Briefly, there was a ^{99m}Tc labeled blood with and without RRx-001 observed in the bladder and liver compared to other organs. These results, while unsurprising, suggest that most RRx-001 modified RBCs were observed to undergo hepatic elimination and some renal

(A)   (B)
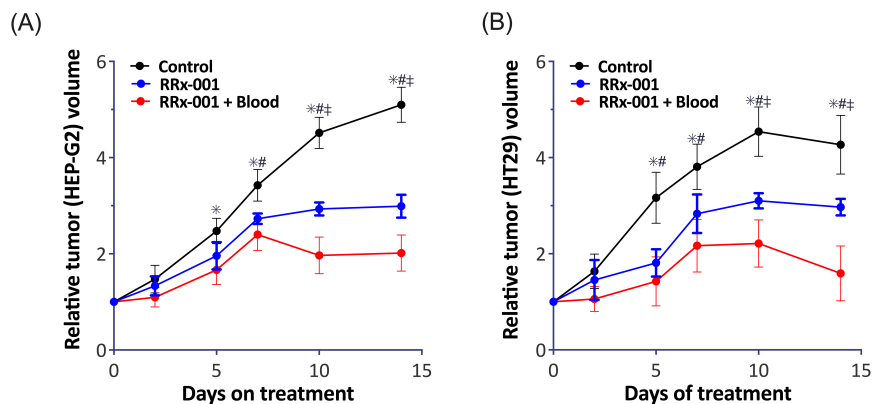
Figure 2.4: RRx-001 Treated RBCs Augment Tumor Cytotoxicity Compared with RRx-001 treatment alone. Shown here is the relative tumor volume in both our **(A)** HEP-G2 and **(B)** HT29 tumor models after treatment with vehicle (black), RRx-001 alone (blue), and RRx-001 treated RBCs, denoted here as RRx-001 + Blood (red). We observed a significant reduction in both tumor models after treatment with both RRx-001 and RR-001 + blood compared to vehicle control. After 10 days, RRx-001 + blood have an even greater reduction in tumor volume compared with RRx-001 alone. (* p < 0.05 Control vs. RRx-001, # p < 0.05 Control vs. RRx-001 + Blood, ‡ p < 0.05 RRx-001 vs. RRx-001 + Blood).

clearance (Figure 2.3A), presumably modified RBCs were cleared in the liver, while hemoglobin in the kidneys, which was consistent with previous reports of RRx-001 pharmacodynamics [87]. In both tumor models, we observed a dose dependent and significant increase (p < 0.05 compared to vehicle) in %RRx-001 injected in both tumor models as assessed by fraction of ^{99m}Tc radiolabeled RBCs (Figure 2.3B). Total body radioactivity (Figure 2.3C) was observed to decrease with increasing dose of RRx-001 (p < 0.05 at 10 mg/kg compared to vehicle) likely as we are underestimating the volume of treated RBCs in the tumor due to competition between ^{99m}Tc and RRx-001 Hb binding. Together these results suggest that RRx-001 treated RBCs preferentially localize to tumors in our experimental models.

We next investigated tumor viability after treatment with RRx-001. First, we observed an approximate 40% and 36% decrease in HEP-G2 and HT-29 tumor weight, respectively, following administration of RRx-001 treated RBCs. We then measured tumor viability over time with treatment of RRx-001 alone and RRx-001 treated RBCs (Figure 2.4) in both HEP- G2 and HT-29 tumor models. Specifically, in HEP-G2 cells, there was a significant reduction in tumor volume

after treatment with RRx-001 treated blood and RRx-001 alone compared with control 7 days post treatment. At 10- and 15-days post treatment, the group treated with RRx-001 treated blood showed a significant reduction in tumor volume compared to treatment with RRx-001 alone. A similar trend was observed in the HT29 tumor model. In summary, we observed that RRx-001 treated RBCs resulted in a significant reduction ($p < 0.05$) in tumor weight in both models compared to vehicle control and treatment with RRx-001 alone after 10 days. Importantly, treatment with RRx-001 alone resulted in a significant reduction in tumor volume ($p<0.05$) compared to vehicle control, but it appears that RBCs treated with RRx-001 augmented tumor cytotoxicity, consistent with what we previously reported [27]. Together, these results further demonstrated that RRx-001 treated RBCs are more cytotoxic to tumor cells compared with RRx-001 alone.

2.4   Discussion

The principal findings of this study are: (1) RRx-001 localizes to RBCs likely by associating with cysteine residues on Hb, (2) RRx-001 treated RBCs preferentially localize to tumors by increasing RBC adhesion to the tumor endothelium in our experimental tumor models, likely by increasing phospholipid phosphatidylserine expression, and (3) localization of RRx-001 treated RBCs affects tumor viability. Importantly, this study demonstrates that RRx-001 treatment of RBCs produces sufficient membrane PS expression to increase RBC adhesion in cases when endothelial PSR expression is increased (e.g., after treatment with TNFα and hypoxia). Further-more, based on this proposed mechanism, an RRx-001 dependent increase in RBC adhesion is independent of tumor cell lineage, as observed in our study.

We observed that ^{99m}Tc incorporation in the insoluble fraction of RBCs decreased with increased RRx-001 dose, suggesting that RRx-001 displaced radiolabeled ^{99m}Tc, which is known to bind to cysteine residues of Hb. These results suggest that RRx-001 preferentially interacts with the insoluble protein fraction, namely Hb, of RBCs, and interacts with Hb cysteine

residues further demonstrating the distinct affinity RRx-001 has for RBCs. [99m] Tc is known to interact preferentially with thiol containing residues (e.g., cysteine) on the beta chain of hemoglobin [84, 88]. RRx-001 is known to interact with similar cysteine residues, and in fact, is known to specifically bind to the cysteine 93 residues on the beta chain of hemoglobin with exquisite specificity [81]. Whether cysteine 93 binding is the predominant mechanism of [99m] Tc displacement in this assay is unknown; RRx-001 may in fact bind other cysteine residues in hemoglobin, further displacing [99m] Tc. Importantly, the association between RRx-001 and cysteine 93 residues accounts for only 10–30% of RRx-001-human Hb interactions, suggesting that interactions with GHS and other thiolate containing groups within the erythrocyte may in fact account for the majority of the drug's oxidative effects in RBCs [81]. Subsequent NO production during hypoxia may be both from RRx-001's interactions with cysteine 93 residues and other antioxidants (e.g., GSH) within the erythrocyte [81, 83]. The observed preferential localization of RRx-001 to RBCs in our study suggests that oxidation and depletion of the intra-erythrocyte GSH pool may be the predominant mechanism of RRx-001 mediated cytotoxicity. Furthermore, depletion of GSH by RRx-001 severely limits the erythrocyte's ability to reduce reactive oxygen species (ROS) formation, further increasing the probability of Hb oxidation [81].

The results from our study further support the hypothesis that RBCs are the critical effector of cytotoxicity after RRx-001 treatment. As discussed above and demonstrated by several studies [27, 81], RRx-001 mediated cytotoxicity and chemosensitization depends on increased RBC oxidation and NO production. Several mechanisms for NO production exist, though most relevant here are NO production from βcys93 residue interactions and interactions with and depletion of GSH (and other antioxidant species) [27, 81]. Important to our study, however, is the idea that increased Hb oxidation results in translocation of PS on the outer membrane of the RBC. Such a translocation has several implications, including increased RBC aggregation, discussed in detail below, and decreased tumor viability by means of occlusion of the hypoxic tumor vasculature [27]. This mechanism is further supported by our observation that RRx-001 directly increases PS

expression on the erythrocyte membrane. Vascular occlusion also induces a subsequent vascular normalization from shunting and redirection of blood flow through more efficient vessels, leading to the chemo-sensitization and radio-sensitization commonly observed with RRx-001 treatment. RBCs are then endocytosed by the tumor endothelium, resulting in the release of iron and free heme, which increases oxidative stress. Free heme as well as RRx- 001 mediated downregulation of CD47 expression on tumor cells and SIRPα expression on macrophages induces a shift from the low phagocytic M1 phenotype to the high phagocytic M2 phenotype in tumor cells [27, 28]. Thus, RRx-001 mediated RBC PS externalization may be of pivotal importance to the function of RRx-001 as a chemosensitizer and as a therapeutic for cancer treatment.

Our results show that RRx-001 increases RBC adhesion to the endothelium under TNFα induced inflammation and hypoxia, which explain the observed preferential localization to tumor cells. We hypothesize that the mechanism of increased adhesion is a consequence of an RRx-001 mediated increase in erythrocyte membrane PS and increased interaction with PSR on the endothelium. To induce PSR expression on HUVECs, we utilized TNFα and LPS, both of which are known to stimulate endothelial PSR expression [22]. These effects likely underestimate the true effects RRx-001 on RBC adhesion in vivo, as free heme release from RRx-001 treated RBCs can upregulate PSR after interaction with macrophages, which were not included in our assay. Interestingly, we observed a differential response in changes in RBC adhesive potential with TNFα and LPS, namely that RRx-001 significantly increased adhesion only with TNFα stimulation. These results, are, however, not unexpected, as TNFα is a more potent stimulator of PSR expression in the endothelium compared to LPS, though we admit that the differences in RRx-001 dose may also explain these results [22]. Importantly, treatment of endothelium with TNFα and LPS requires activation of PS expression on RBCs to increase adhesion, further suggestion that our results are explained by an increase in PS-PSR interactions following RRx-001 treatment [22]. The requisite presence of TNFα, which is presumably more abundant in tumor vs. non-tumor endothelium perhaps explains the absence of RRx-001-related side effects in treated

vasculopathic patients with cancer. Future studies should aim to further elucidate these effects.

2.4.1 Limitations

Our study has several limitations. ^{99m} Tc can bind to imidazole rings in histidine residues, which are abundant in Hb [88]. As a result, ^{99m} Tc radiolabeling in general may underestimate the extent to which RRx-001 binds and interacts with thiol containing residues in Hb, though this is a limitation of the assay. Furthermore, the competition between radiolabeled ^{99m} Tc and RRx-001 for cysteine residues on Hb results in an underestimation of the number of RBCs present within the tumor vasculature, as there are fewer ^{99m} Tc labeled RBCs with increasing RRx-001 dose. We also did not directly measure proteins directly indicative of tumor cell death. Given that several apoptotic pathways exist, future studies should measure these proteins to better understand the mechanism by which RRx-001 induces tumor cell death. In our adhesion studies, we did not directly determine measure PSR expression, though we did measure PS expression post RRx-001 treatment. Our results remain speculative as to whether increased PS-PSR interactions are a viable mechanism for the observed increase in RBC adhesion. Future studies should aim to further investigate the specific mechanism of RRx-001 induced increase of PS expression on erythrocyte membranes and further elucidate downstream effects.

2.5 Conclusions

In summary, we showed that RBCs treated with RRx-001 preferentially adhere in tumors, likely due to increased RBC membrane PS expression secondary to an increase in Hb oxidation. RRx-001 treated RBCs demonstrated increased adhesive potential to endothelial cells upon introduction of TNF-α and hypoxia, suggesting that the process is indeed PS-PSR mediated. Future studies should aim to further elucidate the mechanisms by which PS expression is increased in RRx-001 and whether other mechanisms of an RRx-001 mediated increase in RBC adhesion

to the tumor endothelium exist.

Chapter 2, in full, contains material as it appears in RRx-001 Increases Erythrocyte Preferential Adhesion to the Tumor Vasculature. Jani, V. P., Asaro, R., Oronsky, B., and Cabrales, P. (2021). International journal of molecular sciences 22.9 (2021): 4713. The thesis author was the primary investigator and author of this paper.

Chapter 3

NO Nanoparticles Reduce Inflammation in a Small Animal Model of ARDS

Abstract: Acute respiratory distress syndrome (ARDS), hallmarked by high permeability pulmonary edema and hypoxemic respiratory failure, is associated with high morbidity and mortality. Current treatment protocols rely on improving O_2 delivery, decreasing O_2 consumption, and treating the underlying cause of the initial insult. We hypothesize that targeting molecular mediators of inflammation in ARDS by exogenous supplementation of highly bioavailable nitric oxide nanoparticles (NO-nps) may improve hypoxemia and reduce neutrophil mediated inflammation in ARDS. We used a small rodent model of ARDS by inducing lung injury with inhalation of lipopolysaccharide (LPS; 0.5 μg LPS/ L) with LPS derived Escherichia coli O55: B5 Sigma, 3,000,000 EU/mg administered at 100 mL/min. Three different treatments were given to different groups, inhaled NO at 70 ppm, inhaled NO at 140 ppm, and NO-nps and compared with untreated rodents, 72 hours after initial insult. NO-nps were suspended in PBS (1 mg/mL) and nebulized at 60 mL/min for 30 min. Concurrent with treatment, the fraction of inspired O_2 was increased after 30 minutes from 21% to 40% and finally from 40% to 60%. At an FiO_2 of 60% and 72 hours post induction of ARDS, NO-np treated mice had an arterial pO_2 (PaO2) of 142 $\pm$ 9 mmHg, significantly higher than mice treated with inhaled NO at 70 ppm (87 ± 5 mmHg, p=8.4×10^{-8}) and inhaled NO at 140 ppm (107 ± 6 mmHg, p=6.1×10^{-6}). Neutrophils in both the periphery ($1.6\times10^5 \pm 0.4 \times 10^5$ cells) and bronchoalveolar lavage fluid (BALF; $2.7\times10^5 \pm 0.8 \times 10^5$ cells) were significant reduced in NO-np treated mice compared

to mice treated with inhaled NO at 70 ppm (p=0.0097, $2.4 \times 10^5 \pm 0.5 \times 10^5$ cells for periphery, p=0.0075, $3.8 \times 10^5 \pm 0.8 \times 10^5$ cells for BALF). In summary, we found that treatment with NO-np improved arterial PO_2 at a high FiO_2 compared to inhaled NO alone and that NO-nps reduced both circulating and pulmonary interstitial neutrophil count, while inhaled NO did not. Future studies should aim to elucidate the precise mechanisms behind how NO-nps mediate neutrophilic inflammation in ARDS. In addition, our study provides preliminary evidence that NO-nps may improve outcomes in patients with ARDS by reducing inflammation and should be considered for future clinical assessment.

Keywords: Acute Respiratory Distress Syndrome, Nitric Oxide, Lipopolysaccharide, NO nanoparticles

3.1   Introduction

Acute Respiratory Distress Syndrome (ARDS) is a syndrome of respiratory distress within 7 days of insult or new symptoms characterized by high permeability pulmonary edema and acute hypoxemic respiratory failure [29, 30]. Importantly, pulmonary edema in ARDS is non-cardiogenic and is associated with increased permeability of the alveolar-epithelial and alveolar-endothelial barrier [89]. Classically, ARDS is thought to progress from injury by infection, trauma, or other exogenous cause (e.g., transfusion associated lung injur[90], with bacterial or viral pneumonia being the most common etiology [91]. The pathogenesis of ARDS involves dysregulated, maladaptive inflammatory cascades in response to infection or trauma, which subsequently increases alveolar membrane permeability and induces diffuse alveolar damage (DAD) [91]. Ultimately, this results in extravasation of fluid to the extravascular space, leading to interstitial and alveolar edema, a so-called permeability pulmonary edema [91]. Thus, ARDS can be thought of as a maladaptive inflammatory response akin to sepsis, with alveolar membrane permeability being the primary driver of disease pathogenesis.

The mechanisms of hypoxemia in ARDS primarily result from right to left intrapulmonary

shunt and ventilation-perfusion (V/Q) mismatch, the latter explaining the perceived benefit from increasing fraction of inspired O_2 (FiO_2). Accumulation of fluid secondary to increased alveolar permeability increases the work for breathing, which decreases pulmonary compliance and reduces ventilated lung volume, and induces atelectasis, thereby resulting in intrapulmonary shunts and V/Q mismatch in transition zones. Moreover, alveolar fluid clearance (AFC) in ARDS is greatly reduced, which only worsens pulmonary edema and pulmonary function in these patients [32]. The reduction in AFC is thought to result from hypoxia and hypercapnia, with subsequent impairment in Na-K/ATPase function, increased tidal volumes, elevated airway pressures, and pro-inflammatory cytokines, all of which serve to injure the alveolar epithelium and impair osmotic gradients necessary for fluid transport [32].

Further alveolar damage in ARDS is thought to result from direct injury by dysregulated inflammatory pathways, often driven by pathogen associated molecular patterns binding to toll-like receptors on lung epithelium and alveolar macrophages, which activate neutrophils, the predominant mediator of inflammation in ARDS [32]. Recently however, several studies have identified that significant insult to the pulmonary vascular endothelium presents as a significant driver of local inflammation in ARDS [92, 93]. Nonetheless, current treatments for ARDS involve reducing shunt fraction, reducing atelectasis, and improving pulmonary compliance with positive end expiratory pressure (PEEP), increasing O_2 delivery, decreasing O_2 consumption, and treating the underlying cause of the initial insult.

Targeting the molecular mediators of inflammation and endothelial injury in ARDS may help to improve outcomes compared to ventilatory support alone. Nitric oxide (NO), known for maintaining the vascular endothelium and regulating inflammatory cascades associated with microvascular injury and sepsis, has been of interest, particularly in ARDS. Historically, while small clinical trials have demonstrated improved arterial oxygenation, decreased pulmonary hypertension, and decreased need for ventilatory support with NO inhalation, the effects were modest [94, 95]. Here, we sought to investigate whether novel technologies that improve NO

47

bioavailability and half-life, namely NO nanoparticles (NO-nps) [96], can be used to downregulate inflammation in a rodent model of ARDS. Specifically, we induced an ARDS-like inflammatory phenotype by inhalation of lipopolysaccharide (LPS) and subsequently treated with either inhaled NO or NO-nps. We demonstrated that in addition to improved arterial oxygen saturation, NO-nps reduce both pulmonary and systemic neutrophils, the predominant mediator of inflammation in ARDS, supporting its potential clinical utility.

3.2 Materials and Methods

3.2.1 ARDS Animal Model.

Mice (Jackson Labs, Bar Harbor ME) were exposed to 0.5 μg LPS/ L in 1-hour increments by nasal inhalation. LPS treatment was repeated every 24 hours to maintain the inflammatory phenotype. For all animals in this study, the NIH Guide for the Care and Use of Laboratory Animals was followed. The study protocol was approved by the local animal care committee. The LPS used in this study was derived from Escherichia coli O55: B5 Sigma, 3,000,000 EU/mg. LPS aerosolization was achieved via an aerosol nebulizer device at 100 mL/min. The dose of LPS given was controlled by adjusting the solution strength of LPS in liquid.

3.2.2 Nebulized NO-nps.

Production of the NO releasing nanoparticles (NO-nps) used in this study was previously described [97, 98, 99]. These particles were shown [100] to be effective as as an IV infusion method to deliver NO systemically. IV systemic infusion of these NO releasing particles was shown to be highly effective in controlling systemic inflammation from multiple triggers including HBOC induced toxicity [101], hemorrhagic shock [102] and LPS induced endotoxic shock [103].

3.2.3 Experimental Protocol – Nebulized NOnp and Inhaled NO.

Three different treatments were given to different groups, NO at 70 ppm, inhaled NO at 140 ppm, and NO nanoparticles (NO-nps). Treatments were given 72 hours after the initial exposure to LPS regardless of treatment type/group. Inhaled NO at 70 and 140 ppm were produced by mixing O2 and N2. No-nps were suspended in PBS (1 mg/mL) and nebulized at 60 mL/min for 30 min. Concurrent with treatment, the fraction of inspired O2 was increased after 30 minutes from 21 % to 40 % and finally from 40 % to 60 %.

3.2.4 Statistical Analysis.

All data are represented as mean $\pm$SD. Oxygen saturation, partial pressure, and lactate data were compared using a two-way repeated measures analysis of variance (RM-ANOVA) with row and column factors being time after induction of ARDS/after NO treatment and treatment group, respectively. When appropriate, post hoc analysis was performed with Holm-Sidak multiple comparisons for parametric data. Inflammatory cell counts and systemic cytokines were compared using ordinary one-way ANOVA, with assumed normality given the distribution and sample size of the data, and equal variances confirmed with a Brown-Forsythe test. When appropriate, post hoc analysis was performed with Holm-Sidak multiple comparisons for parametric data. All statistical analysis performed in GraphPad Prism 9.1 (GraphPad Software, San Diego, CA). Changes were considered significant if p values were < 0.05.

3.3 Results

3.3.1 NO-np Improves Arterial Oxygen Saturation in ARDS.

ARDS was induced by treatment with aerosolized LPS. 24 hours following induction of ARDS, mice were treated with either NO-np or one of two doses of inhaled NO (70 ppm or 140 ppm), n=8/group. 72 hours following treatment, mice were provided escalating doses
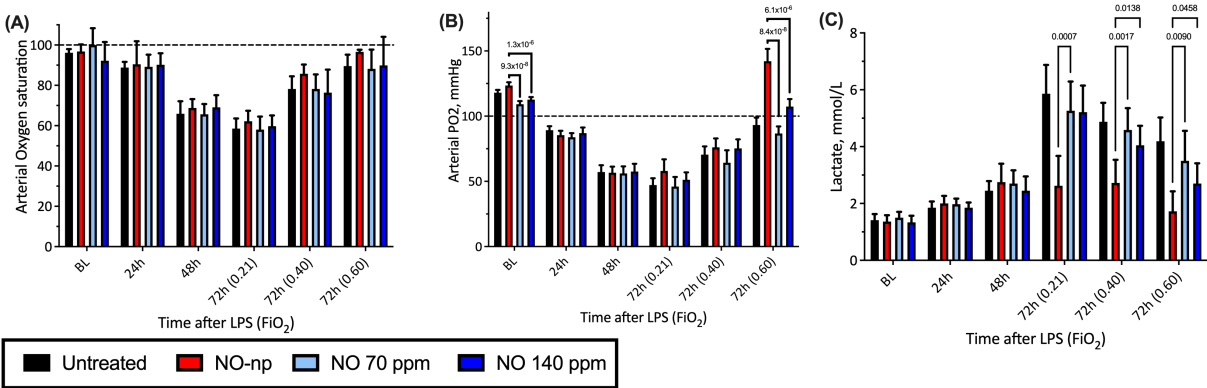
Figure 3.1: Arterial Oxygen Saturation, pO$_2$, and Lactate post NO Treatment. (A) Arterial oxygen saturation, (B) Arterial pO$_2$, and (C) Lactate post treatment with inhaled NO and NO-np. Results were compared with 2-Way ANOVA Tukey's multiple comparisons when appropriate.

of FiO$_2$ (0.21, 0.40, or 0.60) in 30$-$minute increments. Arterial oxygen saturation, arterial pO$_2$, and lactate for all treatment groups and all FiO$_2$ are summarized in Figure 3.1. Briefly, 2-way RM-ANOVA revealed no significant differences in arterial oxygen saturation between all treatment groups ($p = 0.086$), with differences only attributed to either the induction of ARDS or time post treatment ($p = 1 \times 10^{-15}$). For arterial pO$_2$, 2-way RM-ANOVA revealed significant differences due to both treatment group ($p = 1 \times 10^{-15}$) and time post treatment ($p = 1 \times 10^{-15}$). Specifically, post-hoc analysis revealed a significant increase in arterial PO2 in the NO-np group compared to groups treated with 70 ppm inhaled NO ($p = 8.4 \times 10^{-8}$) and 140 ppm inhaled NO ($p = 6.1 \times 10^{-6}$) at an FiO$_2$ of 0.60 72 hours post treatment. Surprisingly, no significant differences were observed in arterial pO$_2$ between all groups at all other time points and lower FiO$_2$ (Figure 3.1B), suggesting that neither NO-np nor inhaled NO completely corrected ventilation-perfusion (VQ) mismatch responsible for hypoxemia in this model. Serum lactate, reflective of the degree of systemic hypoxia from increased anaerobic metabolism, is summarized in Figure 3.1C. Briefly, 2-way RM-ANOVA revealed significant differences due to both treatment group ($p = 1 \times 10^{-15}$) and time post treatment ($p = 1 \times 10^{-15}$). Consistent with measured arterial pO$_2$, serum lactate was also significantly depressed in the NO-np group (p=0.0090 vs. 70 ppm inhaled NO, p = 0.0458 vs. 140 ppm inhaled NO).
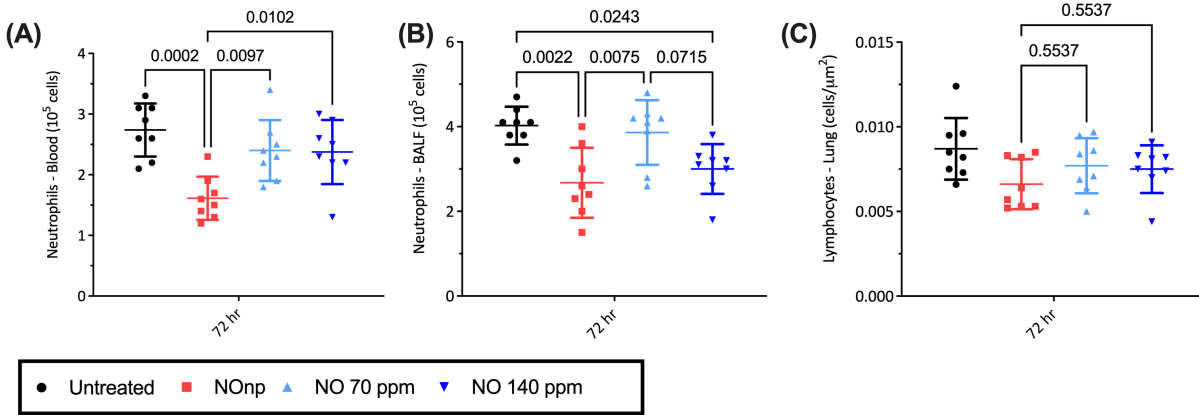
Figure 3.2: Blood and BALF Neutrophil and Lymphocyte Counts. (A) Blood neutrophil, (B) BALF neutrophil, and (C) BALF lymphocyte counts post treatment with inhaled NO and NO-nps. Results were compared with one-way ANOVA with Tukey multiple comparisons when appropriate.

3.3.2   NO-np Reduces Inflammation in ARDS

. To assess the degree of inflammation, the predominant mediator of inflammation in ARDS, neutrophils, were assessed in the peripheral and bronchoalveolar lavage fluid (BALF), reflective of neutrophilic infiltration in the pulmonary interstitium (Figures 3.2A,3.2B). Briefly, peripheral neutrophils were significantly reduced solely in the NO-np group compared to all other treatment groups (p=0.0002 vs. untreated, p=0.0097 vs. 70 ppm inhaled NO, p=0.0102 vs. 140 ppm inhaled NO). In the BALF, neutrophils were reduced in both the NO-np treatment group (p=0.0022) and 140 ppm inhaled NO group (p=0.0243) compared to untreated mice. In addition, BALF neutrophils were reduced in the NO-np group compared to the 70 ppm inhaled NO group (p=0.0075) but not the 140 ppm inhaled NO group (p=0.7694). Lymphocytes were next assessed in the lung parenchyma (Figure 3.2C), and no significant differences were observed between all groups, supporting that our animal model of ARDS mimics the acute inflammatory phenotype classically seen. We next assessed serum cytokines associated with an acute phase reaction and acute inflammation, namely IL-1β, IL-6, and TNFα. Briefly, no significant differences were observed in either systemic or BALF inflammatory cytokines between groups, with the exception
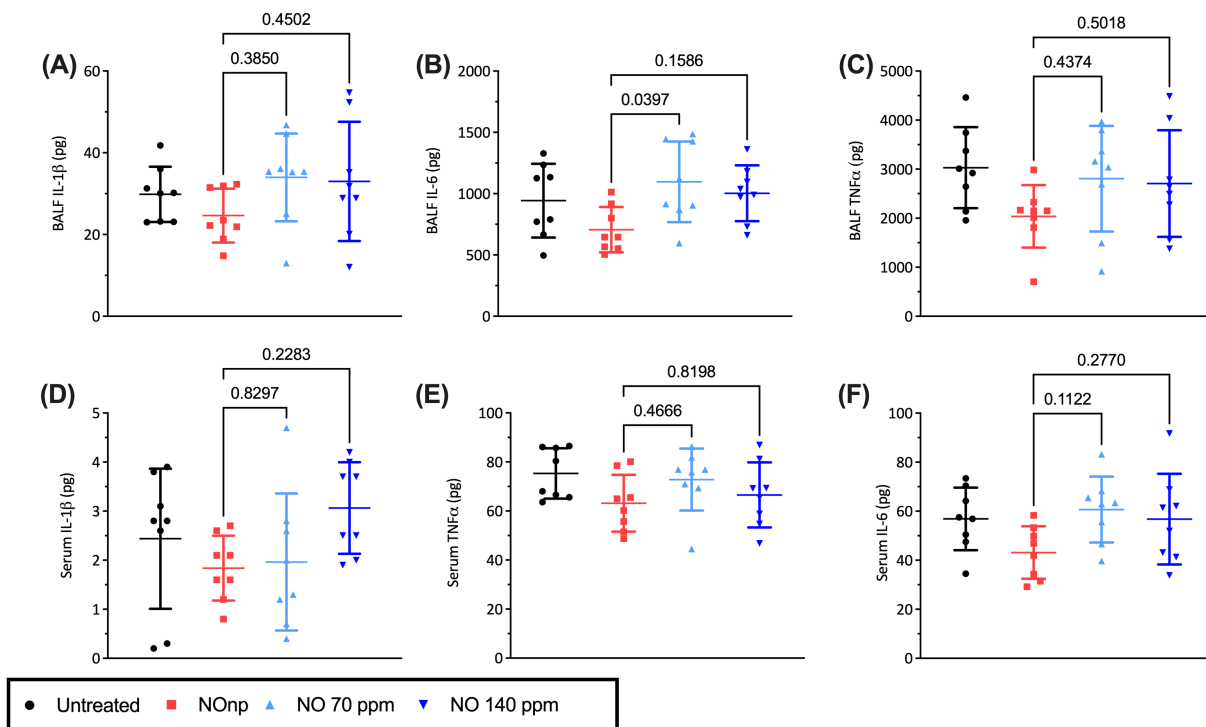
Figure 3.3: Serum and BALF Inflammatory Cytokines. (A) IL-1β, (B) IL-6, and (C) TNFα measured from the BALF post treatment with NO-nps and inhaled NO. (D) IL-1β, (E) IL-6, and (F) TNFα from the serum post treatment with NO-nps and and inhaled NO.

of decreased BALF IL-6 in the NO-np treated group vs. the 70-ppm inhaled treated group (p=0.0397). Detailed post-hoc comparisons and levels of inflammatory cytokines are summarized and presented in Figure 3.3.

3.4   Discussion

.

This study evaluates the efficacy of NO-nps, a more efficient and bioavailable delivery vehicle for NO, to treat neutrophilic inflammation in a small animal model of ARDS. The principal findings of our study are that treatment with NO-nps improved arterial PO2 at high FiO2 compared to inhaled NO alone and that NO-nps reduced both circulating and pulmonary interstitial neutrophil count, while inhaled NO did not. These data suggest that the increased

bioavailability afforded by the nanoparticle delivery vehicle for NO attenuates inflammation both in the lung parenchyma and in the pulmonary capillary endothelium in ARDS providing insight into the molecular mechanism for NO-nps for ARDS treatment.

As stated, our study demonstrated an improvement in arterial pO_2 with NO-nps at high FiO_2 to near baseline levels. Importantly, while a high dose (140 ppm) of inhaled NO produced a similar result, arterial pO_2 was higher in those mice treated with NO-nps. Broadly, hypoxemia results from right-to-left intrapulmonary shunt, V/Q mismatch, diffusion impairment, and hypoventilation [104]. In ARDS, atelectasis and permeability pulmonary edema result in shunt and V/Q mismatch being the primary mediators of hypoxemia. Of these physiologic mechanisms, only V/Q mismatch can be improved with increasing the alveolar-arterial gradient (A-a). Thus, pulmonary pathologies with V/Q mismatch as the primary mediator of hypoxemia (e.g., ARDS) will see increase arterial pO_2 with increasing FiO_2 [30, 29]. Provided this mechanism, we hypothesize that the significant improvement of arterial pO_2 in NO-np treated ARDS suggests that NO-np improves V/Q mismatch in ARDS, likely by reducing transition zones between atelectatic and normal lung.

Inflammation in ARDS results in damage to both the alveolar epithelium and the pulmonary capillary endothelium. In ARDS, the former is thought to be mediated by neutrophilic migration, which induces epithelial injury and apoptosis and thus increased epithelial-alveolar permability [32, 105]. In our study, we observed a decreased neutrophil count (both in the periphery and the pulmonary interstitium) in those mice treated with NO-np but not those treated with inhaled NO, suggesting that the increased bioavailability and half-life of NO in the nanoparticle suspension is able to directly target neutrophil mediated inflammatory mechanisms associated with epithelial injury in ARDS [106, 107]. Improvement in alveolar epithelial function likely also contributes to improvements in hypoxemia, as demonstrated in our model. Surprisingly, other than IL-6 in the BALF, the acute phase reactants IL-6 and IL-1β did not improve with treatment, potentially suggesting that NO-nps do not mediate the acute phase response. Future studies should aim to investigate neutrophil chemotactic mediators (e.g., IL-8) [106, 107] post treatment with NO-nps

as a potential mediator of inflammation.

As alluded to above, the vascular endothelium is significantly injured in ARDS and is likely one of the predominant mediators of disease [93]. Essential to alveolar endothelial integrity is vascular endothelial (VE) cadherin. Lung injury, as in ARDS, results in increased TNFα, vascular endothelial growth factor, and leukocyte signaling, which is known to destabilize VE cadherin bonds, thereby impairing endothelial structural integrity and fucntion [32, 108]. In fact, one prior study demonstrated that in the same LPS model of mouse ARDS used in our study, genetically stabilizing VE cadherin bonds resulted in reduced pulmonary edema, suggesting that VE cadherin injury secondary to inflammation is indeed a primary mediator of permeability pulmonary edema in ARDS [32, 108]. More recently, inflammation in ARDS was known to alter endothelial glycocalyx structure and function, further worsening disease pathogenesis [92, 93]. Together, the insult to both VE cadherin and the glycocalyx ultimately deplete vascular NO, resulting in persistent inflammation, reduced tissue O_2 delivery, and reduced waste removal through the hypoxic lung parenchyma in ARDS [92, 93, 109]. Our study reveals that delivering NO in the highly bioavailable NO-np form improves hypoxemia, reduces anaerobic respiration, and reduces inflammation associated with ARDS. We hypothesize that the results in our study likely result from the vasoprotective role of NO, and that delivery of NO-np improves vascular endothelial structure and integrity. Furthermore, based on studies demonstrating the endothelial glycocalyx protective effects of NO in the coronary vasculature [110], we further posit that the effects of NO will prevent further vascular insult in ARDS. Surprisingly, our studies shows that these effects appear to be TNFα independent, suggesting that high concentrations of NO improve vascular endothelial function by some alternate inflammatory cascade. Future studies should aim to further elucidate mechanisms associated with exogenous NO delivery and improved pulmonary capillary endothelial function in ARDS.

The current results obtained using these inhaled nanoparticles differed partially from the results seen for the IV infusion study on LPS induced endotoxic shock [103]. In both cases

the results showed pronounced anti-inflammatory activity; however, the IV infused particles exhibited a more extensive range of anti-inflammatory consequences with reduction in several cytokine markers that were not noticeably impacted in the current study. A possible explanation is that the impact of IV delivered NO on the endothelial lining on the vasculature may have a different outcome than NO delivered to the epithelial lining of the lungs. Follow up studies to evaluate these differences are being planned. A comparison of the two studies suggests that the most effective therapeutic strategy might be one in which both the vascular endothelium and the pulmonary epithelium are targeted.

The idea of NO for treatment of acute lung injury (ALI) and ARDS is not a new one and has in fact recently gained momentum as a potential treatment for COVID-19 mediated ALI [4]. Specifically in ARDS, treatment with inhaled NO resulted in modest improvements in arterial oxygenation, pulmonary hypertension, and need for ventilatory support [94, 95]. Other studies have demonstrated that treatment with NO is non-inferior compared to standard clinical practice (high FiO2, PEEP, etc.) and other immune suppressants (e.g., corticosteroids) [111]. We hypothesize that relatively modest effects of NO result from its short half-life and poor bioavailability, being a small gaseous molecule. To this end, we specifically investigated a novel delivery vehicle for NO, NO-nps. NO-nps have recently gained traction for a variety of clinical applications due in part to their use as a controlled delivery vehicle, improved bioavailability, and potential scalability [96]. Currently, few FDA approved inhaled NO delivery mechanisms exist, namely Bellerophon Therapeutics INOpulse and VERO Biotech's GENOSYL DS iNO [112], and to our knowledge, no NO-np based therapeutics are FDA approved. The results from our study suggest that the ability of NO-nps to improve neutrophilic mediated inflammation in ARDS make them an attractive supplement to mechanical ventilation and should be considered for clinical assessment in future studies.

3.4.1 Limitations

Our study has several limitations. We did not directly measure either serum or pulmonary interstitial NO levels in all groups, which is of interest in future studies. In addition, the animal model used in our study effectively models ARDS secondary to bacterial pneumonia, as LPS is the primary stimulant, and whether the results apply to other forms of ARDS is yet to be considered. Finally, to address inflammation in our study, we only measured acute phase reactant cytokines and cell counts and no other known mediators of neutrophils chemotaxis. Future studies should aim to investigate the generalizability of our findings to several etiologies of ARDS as well as the precise mechanisms by which treatment with NO-nps mediates inflammation in ARDS.

3.5 Conclusion

In summary, we investigated NO-np treatment in a small animal model of ARDS, induced by direct inhalation of LPS. Our results demonstrate that compared to inhaled NO, NO-np treatment improves hypoxemia, reduces tissues hypoxia, as assessed by serum lactate, and attenuates neutrophil mediated inflammation, which is a hallmark of ARDS. We hypothesize that the benefits of NO-np results from its improved bioavailability and thus enhanced vasoprotective function. Our study also suggests that NO-np may improve outcomes in ARDS and should be considered for future clinical studies. In addition, future studies should better elucidate the mechanism behind which NO-nps improved ARDS associated inflammation.

Chapter 3, in full, is currently being prepared for submission for publication of the material as it appears in Nitric Oxide Nanoparticles Reduce Inflammation in Small Animal Model of ARDS. Jani, V. Friedman, J. Cabrales, P. The thesis author was the primary investigator and author of this paper.

Bibliography

[1] Aleksander S Popel and Paul C Johnson. Microcirculation and hemorheology. *Annu. Rev. Fluid Mech.*, 37:43–69, 2005.

[2] Goksel Guven, Matthias P Hilty, and Can Ince. Microcirculation: physiology, pathophysiology, and clinical application. *Blood purification*, 49(1-2):143–150, 2020.

[3] Amy G Tsai, Pedro Cabrales, Nanae Hangai-Hoger, and Marcos Intaglietta. Oxygen distribution and respiration by the microcirculation. *Antioxidants & redox signaling*, 6(6):1011–1018, 2004.

[4] Nagasai C Adusumilli, David Zhang, Joel M Friedman, and Adam J Friedman. Harnessing nitric oxide for preventing, limiting and treating the severe pulmonary consequences of covid-19. *Nitric Oxide*, 2020.

[5] David D Gutterman, Dawid S Chabowski, Andrew O Kadlec, Matthew J Durand, Julie K Freed, Karima Ait-Aissa, and Andreas M Beyer. The human microcirculation: regulation of flow and beyond. *Circulation research*, 118(1):157–172, 2016.

[6] Etorre Crimi, LJ Ignarro, and C Napoli. Microcirculation and oxidative stress. *Free radical research*, 41(12):1364–1375, 2007.

[7] Jean Davignon and Peter Ganz. Role of endothelial dysfunction in atherosclerosis. *Circulation*, 109(23_suppl_1):III–27, 2004.

[8] An S De Vriese, Tony J Verbeuren, Johan Van de Voorde, Norbert H Lameire, and Paul M Vanhoutte. Endothelial dysfunction in diabetes. *British journal of pharmacology*, 130(5):963–974, 2000.

[9] Ozlem Yalcin, Vivek P Jani, Paul C Johnson, and Pedro Cabrales. Implications enzymatic degradation of the endothelial glycocalyx on the microvascular hemodynamics and the arteriolar red cell free layer of the rat cremaster muscle. *Frontiers in physiology*, 9:168, 2018.

[10] A Corstian, Eva Klijn, Wim K Lagrand, J Jasper Brugts, Can Ince, Peter E Spronk, and Maarten L Simoons. The microcirculation in health and critical disease. *Progress in cardiovascular diseases*, 51(2):161–170, 2008.

[11] Alexandros Rovas, Irina Osiaevi, Konrad Buscher, Jan Sackarnd, Phil-Robin Tepasse, Manfred Fobker, Joachim Kühn, Stephan Braune, Ulrich Göbel, Gerold Thölking, et al. Microvascular dysfunction in covid-19: the mystic study. *Angiogenesis*, 24(1):145–157, 2021.

[12] Jerzy Gebicki, Joanna Katarzynska, and Andrzej Marcinek. Can the microcirculatory response to hypoxia be a prognostic factor for covid-19? *Respiratory Physiology & Neurobiology*, 280:103478, 2020.

[13] Enrique Saldívar, Pedro Cabrales, Amy G Tsai, and Marcos Intaglietta. Microcirculatory changes during chronic adaptation to hypoxia. *American Journal of Physiology-Heart and Circulatory Physiology*, 285(5):H2064–H2071, 2003.

[14] Pedro Cabrales, Amy G Tsai, and Marcos Intaglietta. Microvascular pressure and functional capillary density in extreme hemodilution with low-and high-viscosity dextran and a low-viscosity Hb-based O2 carrier. *American Journal of Physiology-Heart and Circulatory Physiology*, 287(1):H363–H373, 2004.

[15] Bjoern Hussmann, Carsten Schoeneberg, Pascal Jungbluth, Matthias Heuer, Rolf Lefering, Teresa Maek, Frank Hildebrand, Sven Lendemans, and Hans-Christoph Pape. Enhanced prehospital volume therapy does not lead to improved outcomes in severely injured patients with severe traumatic brain injury. *BMC emergency medicine*, 19(1):1–9, 2019.

[16] Brian J Eastridge, John B Holcomb, and Stacy Shackelford. Outcomes of traumatic hemorrhagic shock and the epidemiology of preventable death from injury. *Transfusion*, 59(S2):1423–1428, 2019.

[17] Nicholas Hooper and Tyler J Armstrong. Hemorrhagic shock. *StatPearls [Internet]*, 2020.

[18] Pedro Cabrales, Amy G Tsai, John A Frangos, and Marcos Intaglietta. Role of endothelial nitric oxide in microvascular oxygen delivery and consumption. *Free Radical Biology and Medicine*, 39(9):1229–1237, 2005.

[19] Pedro Cabrales, Marcos Intaglietta, and Amy G Tsai. Transfusion restores blood viscosity and reinstates microvascular conditions from hemorrhagic shock independent of oxygen carrying capacity. *Resuscitation*, 75(1):124–134, 2007.

[20] AE Taylor. Capillary fluid filtration. starling forces and lymph flow. *Circulation research*, 49(3):557–575, 1981.

[21] HS Reinhold and B Endrich. Tumour microcirculation as a target for hyperthermia. *International Journal of Hyperthermia*, 2(2):111–137, 1986.

[22] BN Yamaja Setty and Suhita Gayen Betal. Microvascular endothelial cells express a phosphatidylserine receptor: a functionally active receptor for phosphatidylserine-positive erythrocytes. *Blood, The Journal of the American Society of Hematology*, 111(2):905–914, 2008.

[23] B Lubin, D Chiu, J Bastacky, B Roelofsen, and LL Van Deenen. Abnormalities in membrane phospholipid organization in sickled erythrocytes. *The Journal of clinical investigation*, 67(6):1643–1649, 1981.

[24] Bryan Oronsky, Jan Scicinski, Tony Reid, Arnold Oronsky, Corey Carter, Neil Oronsky, and Pedro Cabrales. Rrx-001, a novel clinical-stage chemosensitizer, radiosensitizer, and immunosensitizer, inhibits glucose 6-phosphate dehydrogenase in human tumor cells. *Discovery medicine*, 21(116):251–265, 2016.

[25] Bryan Oronsky, Tony R Reid, Christopher Larson, Scott Caroen, Mary Quinn, Erica Burbano, Gina Varner, Bennett Thilagar, Bradley Brown, and Angelique Coyle. Replatinum phase iii randomized study: Rrx-001+ platinum doublet versus platinum doublet in third-line small cell lung cancer. *Future Oncology*, 15(30):3427–3433, 2019.

[26] Bryan Oronsky, Neil Oronsky, Jan Scicinski, Gary Fanger, Michelle Lybeck, and Tony Reid. Rewriting the epigenetic code for tumor resensitization: a review. *Translational oncology*, 7(5):626–631, 2014.

[27] Pedro Cabrales, Jan Scicinski, Tony Reid, Frans Kuypers, Sandra Larkin, Marcel Fens, Arnold Oronsky, and Bryan Oronsky. A look inside the mechanistic black box: Are red blood cells the critical effectors of rrx-001 cytotoxicity? *Medical Oncology*, 33(7):63, 2016.

[28] Pedro Cabrales. Rrx-001 acts as a dual small molecule checkpoint inhibitor by downregulating cd47 on cancer cells and sirpa on monocytes/macrophages. *Translational oncology*, 12(4):626–632, 2019.

[29] Matthew Diamond, Hector L Peniston Feliciano, Devang Sanghavi, and Sidharth Mahapatra. Acute respiratory distress syndrome (ards). *StatPearls [Internet]*, 2020.

[30] ARDS Definition Task Force, VM Ranieri, GD Rubenfeld, B Thompson, N Ferguson, and E Caldwell. Acute respiratory distress syndrome. *Jama*, 307(23):2526–2533, 2012.

[31] Matthew Diamond, Peniston Feliciano HL, Devang Sanghavi, and Sidharth Mahapatra. Acute respiratory distress syndrome. *NCBI StatPearls*, 2017.

[32] Laura A Huppert, Michael A Matthay, and Lorraine B Ware. Pathogenesis of acute respiratory distress syndrome. In *Seminars in respiratory and critical care medicine*, volume 40, pages 031–039. Thieme Medical Publishers, 2019.

[33] X Hu, R H Adamson, B Liu, F E Curry, and S Weinbaum. Starling forces that oppose filtration after tissue oncotic pressure is increased. *American Journal of Physiology-Heart and Circulatory Physiology*, 279(4):H1724–H1736, 2000.

[34] J Rodney Levick and C Charles Michel. Microvascular fluid exchange and the revised Starling principle. *Cardiovascular research*, 87(2):198–210, 2010.

[35] Richard M Effros and James C Parker. Pulmonary vascular heterogeneity and the Starling hypothesis. *Microvascular research*, 78(1):71–77, 2009.

[36] Bernhard F Becker, Daniel Chappell, and Matthias Jacob. Endothelial glycocalyx and coronary vascular permeability: the fringe benefit. *Basic Research in Cardiology*, 105(6):687–701, 2010.

[37] J F Murray. Pulmonary edema: pathophysiology and diagnosis. *The International journal of tuberculosis and lung disease*, 15(2):155–160, 2011.

[38] Xavier Monnet, Nadia Anguel, David Osman, Olfa Hamzaoui, Christian Richard, and Jean-Louis Teboul. Assessing pulmonary permeability by transpulmonary thermodilution allows differentiation of hydrostatic pulmonary edema from ALI/ARDS. *Intensive care medicine*, 33(3):448–453, 2007.

[39] H Glenn Bohlen and Julia M Lash. Active and passive arteriolar regulation in spontaneously hypertensive rats. *Hypertension*, 23(6_pt_1):757–764, 1994.

[40] JULIA M Lash, H GLENN Bohlen, and L Waite. Mechanical characteristics and active tension generation in rat intestinal arterioles. *American Journal of Physiology-Heart and Circulatory Physiology*, 260(5):H1561–H1574, 1991.

[41] Paul C Johnson. The myogenic response. In *The resistance vasculature*, pages 159–168. Springer, 1991.

[42] H Glenn Bohlen and Robert W Gore. Comparison of microvascular pressures and diameters in the innervated and denervated rat intestine. *Microvascular research*, 14(3):251–264, 1977.

[43] Michael A Hill and Elizabeth A Ege. Active and passive mechanical properties of isolated arterioles from STZ-induced diabetic rats: effect of aminoguanidine treatment. *Diabetes*, 43(12):1450–1456, 1994.

[44] CARL R Honig, CHARLES L Odoroff, and JAMES L Frierson. Capillary recruitment in exercise: rate, extent, uniformity, and relation to blood flow. *American Journal of Physiology-Heart and Circulatory Physiology*, 238(1):H31–H42, 1980.

[45] Karel Tyml and Alan C Groom. Fourier transform analysis of periodic variations of red cell velocity in capillaries of resting skeletal muscle in frogs. *Microvascular research*, 20(1):9–18, 1980.

[46] D J Lang and B L Johns. Rat venule mechanical characteristics during venous pressure elevation. *American Journal of Physiology-Heart and Circulatory Physiology*, 252(4):H704–H713, 1987.

[47] Artin A Shoukas and H GLENN Bohlen. Rat venular pressure-diameter relationships are regulated by sympathetic activity. *American Journal of Physiology-Heart and Circulatory Physiology*, 259(3):H674–H680, 1990.

[48] Heinz Kerger, Klaus F Waschke, Klaus V Ackern, Amy G Tsai, and Marcos Intaglietta. Systemic and microcirculatory effects of autologous whole blood resuscitation in severe hemorrhagic shock. *American Journal of Physiology-Heart and Circulatory Physiology*, 276(6):H2035–H2043, jun 1999.

[49] Bernhard Endrich, Kazuaki Asaishi, Alwin Götz, and Konrad Meßmer. Technical report—a new chamber technique for microvascular studies in unanesthetized hamsters. *Research in Experimental Medicine*, 177(2):125–134, 1980.

[50] Krianthan Govender, Carlos J Munoz, Alexander T Williams, and Pedro Cabrales. Negative pressure increases MICROVASCULAR perfusion during severe hemorrhagic shock. *Microvascular Research*, page 104125, 2020.

[51] Jonathan S Jahr, Fedor Lurie, Bernd Driessen, Jessica A Davis, Robert Gosselin, and Robert A Gunther. The HemoCue®, a point of care B-hemoglobin photometer, measures hemoglobin concentrations accurately when mixedin vitro with canine plasma and three hemoglobin-based oxygen carriers (HBOC). *Canadian Journal of Anesthesia*, 49(3):243, 2002.

[52] Jacob Rosenblit, Cláudia Regina Abreu, Leonel Nulman Szterling, José Mauro Kutner, Nelson Hamerschlak, Paula Frutuoso, Thelma Regina Silva Stracieri de Paiva, and Orlando da Costa Ferreira Júnior. Evaluation of three methods for hemoglobin measurement in a blood donor setting. *Sao Paulo Medical Journal*, 117(3):108–112, 1999.

[53] Nivaldo R Villela, Amy G Tsai, Pedro Cabrales, and Marcos Intaglietta. Improved resuscitation from hemorrhagic shock with Ringer's lactate with increased viscosity in the hamster window chamber model. *Journal of Trauma and Acute Care Surgery*, 71(2):418–424, 2011.

[54] D Nolte, H Zeintl, M Steinbauer, S Pickelmann, and K Messmer. Functional capillary density: an indicator of tissue perfusion? *International Journal of Microcirculation*, 15(5):244–249, 1995.

[55] Amy G Tsai, Barbara Friesenecker, Michael McCarthy, Hiromi Sakai, and Marcos Intaglietta. Plasma viscosity regulates capillary perfusion during extreme hemodilution in hamster skinfold model. *American Journal of Physiology-Heart and Circulatory Physiology*, 275(6):H2170–H2180, 1998.

[56] Paul E Banwell and Melinda Musgrave. Topical negative pressure therapy: mechanisms and indications. *International Wound Journal: Review*, 1(2):95–106, 2004.

[57] H Kerger, D J Saltzman, M D Menger, K Messmer, and M Intaglietta. Systemic and subcutaneous microvascular Po2 dissociation during 4-h hemorrhagic shock in conscious hamsters. *American Journal of Physiology-Heart and Circulatory Physiology*, 270(3):H827–H836, 1996.

[58] KLFLEM Meßmer, L Sunder-Plassmann, F Jesch, L Görnandt, E Sinagowitz, M Kessler, R Pfeiffer, E Horn, J Höper, and K Joachimsmeier. Oxygen supply to the tissues during limited normovolemic hemodilution. *Research in Experimental Medicine*, 159(3):152–166, 1973.

[59] Julia M Lash and H Glenn Bohlen. Structural and functional origins of suppressed acetyl-choline vasodilation in diabetic rat intestinal arterioles. *Circulation research*, 69(5):1259–1268, 1991.

[60] Jose M Gonzalez-Fernandez and Bard Ermentrout. On the origin and dynamics of the vasomotion of small arteries. *Mathematical biosciences*, 119(2):127–167, 1994.

[61] David R Harder. Pressure-induced myogenic activation of cat cerebral arteries is dependent on intact endothelium. *Circulation research*, 60(1):102–107, 1987.

[62] DAVID R Harder, RICHARD Gilbert, and JULIAN H Lombard. Vascular muscle cell depolarization and activation in renal arteries on elevation of transmural pressure. *American Journal of Physiology-Renal Physiology*, 253(4):F778–F781, 1987.

[63] YANPING Liu, DAVID R Harder, and JULIAN H Lombard. Myogenic activation of canine small renal arteries after nonchemical removal of the endothelium. *American Journal of Physiology-Heart and Circulatory Physiology*, 267(1):H302–H307, 1994.

[64] C R Honig, C L Odoroff, and J L Frierson. Active and passive capillary control in red muscle at rest and in exercise. *American Journal of Physiology-Heart and Circulatory Physiology*, 243(2):H196–H206, 1982.

[65] Jo C Dumville, Robert J Hinchliffe, Nicky Cullum, Fran Game, Nikki Stubbs, Michael Sweeting, and Frank Peinemann. Negative pressure wound therapy for treating foot wounds in people with diabetes mellitus. *Cochrane database of systematic reviews*, 10, 2013.

[66] Chenyu Huang, Tripp Leavitt, Lauren R Bayer, and Dennis P Orgill. Effect of negative pressure wound therapy on wound healing. *Current problems in surgery*, 51(7):301–331, 2014.

[67] N Robert. Negative pressure wound therapy in orthopaedic surgery. *Orthopaedics & Traumatology: Surgery & Research*, 103(1):S99–S103, 2017.

[68] Ola Borgquist, Richard Ingemansson, and Malin Malmsjö. Wound edge microvascular blood flow during negative-pressure wound therapy: examining the effects of pressures from–10 to–175 mmHg. *Plastic and reconstructive surgery*, 125(2):502–509, 2010.

[69] Zhanjun Ma, Zonghuan Li, Kangquan Shou, Chao Jian, Pengcheng Li, Yahui Niu, Baiwen Qi, and Aixi Yu. Negative pressure wound therapy: Regulating blood flow perfusion and microvessel maturation through microvascular pericytes. *International journal of molecular medicine*, 40(5):1415–1425, 2017.

[70] S Muenchow, R E Horch, and A Dragu. Effects of topical negative pressure therapy on perfusion and microcirculation of human skin. *Clinical hemorheology and microcirculation*, 72(4):365–374, 2019.

[71] A Sogorski, M Lehnhardt, O Goertz, K Harati, N Kapalschinski, T Hirsch, A Daigeler, and J Kolbenschlag. Improvement of local microcirculation through intermittent Negative Pressure Wound Therapy (NPWT). *Journal of tissue viability*, 27(4):267–273, 2018.

[72] Bryan Oronsky, Ramasamy Paulmurugan, Kira Foygel, Jan Scicinski, Susan J Knox, Donna Peehl, Hongjuan Zhao, Shoucheng Ning, Pedro Cabrales, and Thomas A Summers Jr. Rrx-001: a systemically non-toxic m2-to-m1 macrophage stimulating and prosensitizing agent in phase ii clinical trials. *Expert opinion on investigational drugs*, 26(1):109–119, 2017.

[73] Shoucheng Ning, Mark Bednarski, Bryan Oronsky, Jan Scicinski, Gordon Saul, and Susan J Knox. Dinitroazetidines are a novel class of anticancer agents and hypoxia-activated radiation sensitizers developed from highly energetic materials. *Cancer research*, 72(10):2600–2608, 2012.

[74] Michelle M Kim, Hemant Parmar, Yue Cao, Susan J Knox, Bryan Oronsky, Jan Scicinski, Theodore S Lawrence, and Christopher D Lao. Concurrent whole brain radiotherapy and rrx-001 for melanoma brain metastases. *Neuro-oncology*, 18(3):455, 2016.

[75] Michelle M Kim, Hemant Parmar, Yue Cao, Priyanka Pramanik, Matthew Schipper, James Hayman, Larry Junck, Aaron Mammoser, Jason Heth, and Corey A Carter. Whole brain radiotherapy and rrx-001: two partial responses in radioresistant melanoma brain metastases from a phase i/ii clinical trial: a tite-crm phase i/ii clinical trial. *Translational oncology*, 9(2):108–113, 2016.

[76] Daniel Morgensztern, Michal Rose, Saiama N Waqar, John Morris, Patrick C Ma, Thomas Reid, Christina E Brzezniak, Karen G Zeman, Arvinda Padmanabhan, and JoAnn Hirth. Rrx-001 followed by platinum plus etoposide in patients with previously treated small-cell lung cancer. *British journal of cancer*, 121(3):211–217, 2019.

[77] SL Brown, JR Ewing, TN Nagaraja, PS Swerdlow, Y Cao, JD Fenstermacher, and JH Kim. Sickle red blood cells accumulate in tumor. *Magnetic Resonance in Medicine: An Official Journal of the International Society for Magnetic Resonance in Medicine*, 50(6):1209–1214, 2003.

[78] Brent L Wood, Donald F Gibson, and Jonathan F Tait. Increased erythrocyte phosphatidylserine exposure in sickle cell disease: flow-cytometric measurement and clinical associations. *Blood*, 1996.

[79] SD Roseff. Sickle cell disease: a review. *Immunohematology*, 25(2):67–74, 2009.

[80] Felice D'Agnillo and Abdu I Alayash. Interactions of hemoglobin with hydrogen peroxide alters thiol levels and course of endothelial cell death. *American Journal of Physiology-Heart and Circulatory Physiology*, 279(4):H1880–H1889, 2000.

[81] Jan Scicinski, Bryan Oronsky, Michael Taylor, Gang Luo, Timothy Musick, Joseph Marini, Christopher M Adams, and William L Fitch. Preclinical evaluation of the metabolism and disposition of rrx-001, a novel investigative anticancer agent. *Drug Metabolism and Disposition*, 40(9):1810–1816, 2012.

[82] Marcel HAM Fens, Sandra K Larkin, Claudia R Morris, Bill Fitch, Jan Scicinski, Bryan Oronsky, and Frans A Kuypers. No or no no, increased reduction of nitrite to nitric oxide by modified red blood cells, 2011.

[83] Barry W Allen, Jonathan S Stamler, and Claude A Piantadosi. Hemoglobin, nitric oxide and molecular mechanisms of hypoxic vasodilation. *Trends in molecular medicine*, 15(10):452–460, 2009.

[84] MM Rehani and SK Sharma. Site of tc-99m binding to the red blood cell: concise communication. *Journal of Nuclear Medicine*, 21(7):676–678, 1980.

[85] Jake C Forster, Wendy M Harriss-Phillips, Michael JJ Douglass, and Eva Bezak. A review of the development of tumor vasculature and its effects on the tumor microenvironment. *Hypoxia*, 5:21, 2017.

[86] Bashar Emon, Jessica Bauer, Yasna Jain, Barbara Jung, and Taher Saif. Biophysics of tumor microenvironment and cancer metastasis-a mini review. *Computational and structural biotechnology journal*, 16:279–287, 2018.

[87] Natarajan Raghunand, Jan Scicinski, Gerald P Guntle, Bhumasamudram Jagadish, Eugene A Mash, Elizabeth Bruckheimer, Bryan Oronsky, and Ronald L Korn. Magnetic resonance imaging of rrx-001 pharmacodynamics in preclinical tumors. *Oncotarget*, 8(60):102511, 2017.

[88] Paul O Zamora and Buck A Rhodes. Imidazoles as well as thiolates in proteins bind technetium-99m. *Bioconjugate chemistry*, 3(6):493–498, 1992.

[89] Laura A Huppert, Michael A Matthay, and Lorraine B Ware. Pathogenesis of acute respiratory distress syndrome. In *Seminars in respiratory and critical care medicine*, volume 40, page 31. NIH Public Access, 2019.

[90] Jürgen Bux and Ulrich JH Sachs. The pathogenesis of transfusion-related acute lung injury (trali). *British journal of haematology*, 136(6):788–799, 2007.

[91] Michael A Matthay, Lorraine B Ware, and Guy A Zimmerman. The acute respiratory distress syndrome. *The Journal of clinical investigation*, 122(8):2731–2740, 2012.

[92] Ryo Uchimido, Eric P Schmidt, and Nathan I Shapiro. The glycocalyx: a novel diagnostic and therapeutic target in sepsis. *Critical care*, 23(1):1–12, 2019.

[93] Eric P Schmidt, Yimu Yang, William J Janssen, Aneta Gandjeva, Mario J Perez, Lea Barthel, Rachel L Zemans, Joel C Bowman, Dan E Koyanagi, and Zulma X Yunt. The pulmonary endothelial glycocalyx regulates neutrophil adhesion and lung injury during experimental sepsis. *Nature medicine*, 18(8):1217–1223, 2012.

[94] Luni Chen, Peng Liu, He Gao, Bing Sun, Desheng Chao, Fei Wang, Yuanjue Zhu, Göran Hedenstierna, and Chen G Wang. Inhalation of nitric oxide in the treatment of severe acute respiratory syndrome: a rescue trial in beijing. *Clinical infectious diseases*, 39(10):1531–1535, 2004.

[95] Rolf Rossaint, Konrad J Falke, Frank Lopez, Klaus Slama, Ulrich Pison, and Warren M Zapol. Inhaled nitric oxide for the adult respiratory distress syndrome. *New England Journal of Medicine*, 328(6):399–405, 1993.

[96] John F Quinn, Michael R Whittaker, and Thomas P Davis. Delivering nitric oxide with nanoparticles. *Journal of Controlled Release*, 205:190–205, 2015.

[97] Adam Friedman and Joel Friedman. New biomaterials for the sustained release of nitric oxide: past, present and future. *Expert opinion on drug delivery*, 6(10):1113–1122, 2009.

[98] Adam J Friedman, George Han, Mahantesh S Navati, Manju Chacko, Leslie Gunther, Alan Alfieri, and Joel M Friedman. Sustained release nitric oxide releasing nanoparticles: characterization of a novel delivery platform based on nitrite containing hydrogel/glass composites. *Nitric oxide*, 19(1):12–20, 2008.

[99] George Han, Adam J Friedman, and Joel M Friedman. Nitric oxide releasing nanoparticle synthesis and characterization. In *Nitric oxide*, pages 187–195. Springer, 2011.

[100] Pedro Cabrales, George Han, Camille Roche, Parimala Nacharaju, Adam J Friedman, and Joel M Friedman. Sustained release nitric oxide from long-lived circulating nanoparticles. *Free Radical Biology and Medicine*, 49(4):530–538, 2010.

[101] Pedro Cabrales, George Han, Parimala Nacharaju, Adam J Friedman, and Joel M Friedman. Reversal of hemoglobin-induced vasoconstriction with sustained release of nitric oxide. *American Journal of Physiology-Heart and Circulatory Physiology*, 300(1):H49–H56, 2011.

[102] Parimala Nachuraju, Adam J Friedman, Joel M Friedman, and Pedro Cabrales. Exogenous nitric oxide prevents cardiovascular collapse during hemorrhagic shock. *Resuscitation*, 82(5):607–613, 2011.

[103] Alexander T Williams, Cynthia R Muller, Krianthan Govender, Mahantesh S Navati, Adam J Friedman, Joel M Friedman, and Pedro Cabrales. Control of systemic inflammation

through early nitric oxide supplementation with nitric oxide releasing nanoparticles. *Free Radical Biology and Medicine*, 161:15–22, 2020.

[104] Malay Sarkar, N Niranjan, and PK Banyal. Mechanisms of hypoxemia. *Lung India: official organ of Indian Chest Society*, 34(1):47, 2017.

[105] Vasiliki Galani, Eleftheria Tatsaki, Maria Bai, Panagiotis Kitsoulis, Marillena Lekka, Georgios Nakos, and Panayiotis Kanavaros. The role of apoptosis in the pathophysiology of acute respiratory distress syndrome (ards): an up-to-date cell-specific review. *Pathology-Research and Practice*, 206(3):145–150, 2010.

[106] Andrew E Williams, Ricardo J José, Paul F Mercer, David Brealey, Dhruv Parekh, David R Thickett, Cecelia O'Kane, Danny F McAuley, and Rachel C Chambers. Evidence for chemokine synergy during neutrophil migration in ards. *Thorax*, 72(1):66–73, 2017.

[107] Satoshi Gando, Takashi Kameue, Naoyuki Matsuda, Atsushi Sawamura, Mineji Hayakawa, and Hirokatsu Kato. Systemic inflammation and disseminated intravascular coagulation in early stage of ali and ards: role of neutrophil and endothelial activation. *Inflammation*, 28(4):237–244, 2004.

[108] Dörte Schulte, Verena Küppers, Nina Dartsch, Andre Broermann, Hang Li, Alexander Zarbock, Olena Kamenyeva, Friedemann Kiefer, Alexander Khandoga, and Steffen Massberg. Stabilizing the ve-cadherin–catenin complex blocks leukocyte extravasation and vascular permeability. *The EMBO journal*, 30(20):4157–4170, 2011.

[109] Pedro Cabrales, Amy G Tsai, John A Frangos, and Marcos Intaglietta. Role of endothelial nitric oxide in microvascular oxygen delivery and consumption. *Free Radical Biology and Medicine*, 39(9):1229–1237, 2005.

[110] Dirk Bruegger, Markus Rehm, Matthias Jacob, Daniel Chappell, Mechthild Stoeckelhuber, Ulrich Welsch, Peter Conzen, and Bernhard F Becker. Exogenous nitric oxide requires an endothelial glycocalyx to prevent postischemic coronary vascular leak in guinea pig hearts. *Critical care*, 12(3):1–11, 2008.

[111] Mahmoud Ammar, Seth Bauer, Stephanie Bass, Madhu Sasidhar, Rory Mullin, and Simon Lam. 713: Comparison of inhaled epoprostenol to inhaled nitric oxide: A non-inferiority study. *Critical Care Medicine*, 42(12):A1532, 2014.

[112] Roham T Zamanian, Charles V Pollack Jr, Michael A Gentile, Moira Rashid, John Christian Fox, Kenneth W Mahaffey, and Vinicio de Jesus Perez. Outpatient inhaled nitric oxide in a patient with vasoreactive idiopathic pulmonary arterial hypertension and covid-19 infection. *American Journal of Respiratory and Critical Care Medicine*, 202(1):130–132, 2020.